Dynamic transcriptome profiles within spermatogonial and spermatocyte populations during postnatal testis maturation revealed by single-cell sequencing

Kathryn J. Grive[1,2], Yang Hu[3], Eileen Shu[1,2], Andrew Grimson[1,4], Olivier Elemento[3], Jennifer K. Grenier[1,2,5], Paula E. Cohen[1,2,5]

[1]Center for Reproductive Genomics, [2]Department of Biomedical Sciences, and [4]Department of Molecular Biology and Genetics, Cornell University, Ithaca, NY 14850; [3]Englander Institute for Precision Medicine, Weill Cornell Medicine, New York, NY

Keywords: spermatogonia, spermatocytes, first-wave spermatogenesis, steady-state spermatogenesis, meiosis, spermatogonial stem cell, SSC, 10X Genomics, testis, mouse, germ cell

[5]Corresponding Authors: J.K. Grenier (jkg47@cornell.edu) and P.E. Cohen (paula.cohen@cornell.edu)

Abstract

Spermatogenesis is the process by which male gametes are formed from a self-renewing population of spermatogonial stem cells (SSCs) residing in the testis. SSCs represent less than 1% of the total testicular cell population, but must achieve a stable balance between self-renewal and differentiation. Once differentiation has occurred, the newly formed and highly proliferative spermatogonia must then enter the meiotic program in which DNA content is doubled, then halved twice to create haploid gametes. While much is known about the critical cellular processes that take place during the specialized cell division that is meiosis, much less is known about how the spermatocytes in the “first-wave” compare to those that contribute to long-term, “steady-state” spermatogenesis. Given the strictly-defined developmental process of spermatogenesis, this study was aimed at exploring the transcriptional profiles of developmental cell stages over the age of the animal. Using a combination of comprehensive germ cell sampling with high-resolution, single-cell-mRNA-sequencing, we have generated a reference dataset of germ cell gene expression. We show that discrete developmental stages possess significant differences in the transcriptional profiles from neonates compared to juveniles and adults. Importantly, these gene expression dynamics are also reflected at the protein level in their respective cell types. We also show differential utilization of many biological pathways with age in both spermatogonia and spermatocytes, demonstrating significantly different underlying gene regulatory programs in these cell types over the course of testis development and spermatogenic waves. This dataset represents the first unbiased sampling of spermatogonia and spermatocytes in the developing testis over developmental age, at

high-resolution, single-cell depth. Not only does this analysis reveal previously unknown transcriptional dynamics of a highly transitional cell population, it has also begun to reveal critical differences in biological pathway utilization in developing spermatogonia and spermatocytes, including response to DNA damage and double-strand breaks.

Author Summary

Spermatogenesis is the process by which male gametes – mature spermatozoa – are produced in the testis. This process requires exquisite control over many developmental transitions, including the self-renewal of the germline stem cell population, commitment to meiosis, and ultimately, spermiogenesis. While much is known about molecular mechanisms regulating single transitions at single time points in the mouse, much less is understood about how the spermatogenic progenitor cells, spermatogonia, or the meiotic cells, spermatocytes, of the testis change over developmental age.

Our single-cell-mRNA-sequencing analysis is the first to profile both spermatogonia and spermatocytes from neonatal mice through adulthood, revealing novel gene expression dynamics and differential utilization of biological pathways. These discoveries help us to understand how the spermatogenic progenitors of this population modulate their activity to adapt to a changing testicular environment. Furthermore, they also begin to explain previously-observed differences - and deficiencies - in spermatocytes that are derived from the first “wave” of spermatogenesis. Overall, this dataset is the first of its kind to comprehensively profile

66 gene expression dynamics in male germ cell populations over time, enriching our
67 understanding of the complex and highly-orchestrated process of spermatogenesis.
68

69 ***Introduction***

70 Mammalian spermatogenesis requires proper establishment of the
71 spermatogonial stem cell (SSC) pool, which resides within the seminiferous tubules of
72 testis and supports life-long germ cell development[1]. These progenitors give rise to all
73 the differentiating germ cells of the mouse testis, ranging from spermatogonia to
74 spermatocytes to spermatids, and finally to mature spermatozoa. Despite the essential
75 nature of this process, the genetic regulatory mechanisms underlying the many complex
76 cellular transitions, and the maturation of this system during testis development, have
77 yet to be fully described.

78 Gamete development in the mouse relies on a rare population of primordial germ
79 cells, the bi-potential progenitors of all gametes, which are specified in the developing
80 embryo at embryonic day (E) 6.25 [2]. These cells migrate to and colonize the developing
81 gonad, arriving at the genital ridge from E10.5 [3], and undergo abundant proliferation
82 until E13.5. At this time, germ cells developing in an XX (female) gonad will enter the
83 meiotic program as oocytes, while germ cells developing in an XY (male) gonad will
84 become prospermatogonia, remaining relatively non-proliferative until shortly after
85 birth[4,5]. Prospermatogonia are able to adopt several fates[6]: in early postnatal life, a
86 subset of these cells differentiate immediately into spermatogonia and continue to
87 progress through spermatogenesis, to constitute the “first wave” of spermatogenesis. A
88 second subset of prospermatogonia will undergo apoptosis, while the remaining

89 prospermatogonia will become established within the testicular stem cell niche soon
90 after birth, to become the self-renewing SSC population that will support “steady-state”
91 spermatogenesis throughout life. This germline stem cell population makes up less than
92 1% of the cells of adult testes[7], and must balance self-renewal and differentiation to
93 maintain a healthy male gamete supply. Thus, the first cohort of meiotically-active male
94 germ cells enter the meiotic program without first entering a self-renewal SSC phase,
95 clearly differentiating the first wave of spermatogenesis from the other subsequent
96 waves.

97 SSCs are triggered to enter spermatogenesis coincident with a burst of retinoic
98 acid (RA), which induces both the spermatogonial divisions and the entry into prophase
99 I of meiosis[8–11]. Thus, in mice, male meiotic entry commences around postnatal day
100 (PND) 10, in response to RA-induced expression of key genes, including ‘Stimulated by
101 Retinoic Acid 8’ (*Stra8*)[8–11]. Spermatocytes execute many essential meiotic events
102 including creation of double-strand breaks, synapsis of homologous chromosomes, and
103 DNA repair and crossover formation, all of which are critical to proper segregation of
104 homologs in the first meiotic division. Failure to properly execute any of these steps is
105 known to result in potential chromosome mis-segregation, non-disjunction events,
106 aneuploidy, and infertility (reviewed comprehensively in [12,13]).

107 While the developmental transitions which underlie germ cell differentiation and
108 maturation have been broadly defined, the gene regulatory underpinnings of these
109 transitions remain largely uncharacterized. Furthermore, studies which have shed some
110 light upon genetic regulatory mechanisms of these processes often focus on single time
111 points, or utilize cell enrichment protocols that may bias the output. In this manuscript,

112 we have performed the first single-cell sequencing developmental time series of the
113 male mouse germline with comprehensive/unbiased sampling, thereby capturing all
114 germ cell types through the progression of postnatal testis maturation. The advent of
115 single cell transcriptomics provides an invaluable tool for understanding gene
116 expression dynamics at very high resolution in a large number of individual cells in
117 parallel. Furthermore, single-cell sequencing reveals heterogeneity and potential
118 plasticity within cell populations, which bulk mRNA sequencing is unable to accomplish,
119 making it an ideal tool for profiling germ cell populations which rapidly progress through
120 myriad developmental transitions.

121 We demonstrate that germ cells display novel gene regulatory signatures over
122 time, while cells positive for single protein markers have the capacity to change
123 dramatically with age, and therefore cells of a particular "identity" may differ significantly
124 from postnatal to adult life. Intriguingly, we have also begun to identify differential
125 expression of genes in critical biological pathways which may contribute to observed
126 differences in the first-wave of spermatogenesis[14,15]. Dissecting the complex dynamics
127 of these developmental transitions can provide critical information about the
128 transcriptional landscape of both SSCs, spermatogonia, and spermatocytes, and the
129 regulatory mechanisms that underlie the formation of a dynamic and functional
130 complement of germ cells to support life-long spermatogenesis.

131

132

133

134

135 ***Results***

136

137 **Single-cell sequencing from testes of different developmental ages robustly**

138 **defines germ cell populations**

139 Mouse testes were collected at several time points, selected to represent distinct stages

140 of germline development: postnatal day (PND) 6 (during SSC specification), PND 14

141 (first appearance of pachytene spermatocytes during the first wave), PND 18

142 (pachytene and diplotene spermatocytes from the first wave present), PND 25

143 (spermatids present) and PND30 (spermatozoa present) (**Figure 1A**) and subjected to

144 single-cell RNAseq. The tissue was dissociated, and the resulting slurry subjected to

145 30% Percoll sedimentation to remove debris. The PND 18 cell suspension was split

146 and processed either with or without Percoll sedimentation as a technical control; due to

147 similarities between libraries, the data from these libraries was thereafter combined

148 (**Figure S1**). Additionally, due to the proportionally high representation of sperm in the

149 adult testis, it was necessary to increase representation of other germ cell types from

150 these samples. To accomplish this goal, an adult testis suspension post-Percoll

151 sedimentation was split in half and either positively magnetically-cell-sorted (MACS) for

152 the cell surface marker THY1, in an attempt to enrich for spermatogonia[16], or negatively

153 MACS-sorted for ACRV1, in an attempt to deplete testicular sperm[17]. While neither

154 strategy can accomplish complete enrichment of spermatogonia or removal of

155 spermatozoa, respectively, both adult libraries had a representative sample of all germ

156 cell types (**Figure 1B**), and are therefore treated as adult replicates in these data. For

157 each single-cell testis suspension, 4-5,000 cells per mouse were processed through the

158 10X Genomics Chromium System using standard protocols for single cell RNA
159 sequencing. Libraries were sequenced to average depth 98M reads; on average, 91%
160 of reads mapped to the reference genome. After standard data processing, we obtained
161 gene expression profiles for approximately 1,200-2,500 cells per library (**Figure 1B, 2A**)
162 with representation of between 2,500-5,000 genes per cell (**Figure S2**), all of which
163 indicates the robustness of the sequencing method, and the comparability to other
164 single-cell studies.

165 Primary cell clusters revealed by Seurat (**Figure S3**) were identified and merged
166 into superclusters (**Figure 2B**) based on known marker gene expression (**Table S1**).
167 While somatic cells were evident in the clustering analysis, including Sertoli cells,
168 smooth muscle, and epithelial and hematopoetic cells, they represent a minority (fewer
169 than 25%) of the total cells profiled. In particular, Sertoli cells were primarily derived
170 from the PND6 library (**Figure** 2) due to their increased representation at that time point,
171 as well as processing steps which effectively removed these cells, which become
172 considerably larger in older mice. Therefore, somatic cells were excluded from all
173 additional analysis, which focused on the spermatogonial and spermatocyte populations
174 in the developing testis. Analysis of differentially expressed genes at each time point
175 identifies known marker genes in each cell type, including *Zbtb16* (*Plzf*), *Sall4*, *Sohlh1*,
176 and *Dmrt1* in spermatogonia; *Meioc*, *Prdm3*, *Top2a*, and *Smc3* in early spermatocytes;
177 *Sycp1/2/3* and *H2afx* in spermatocytes; *Acrv1*, *Izumo1*, and *Catsper3/4* in round
178 spermatids; and *Prm3*, *Izumo3*, and *Tssk6* in elongated spermatids (**Figure 3, S4 & S5,**
179 **Table S1**).

180 Critically, the germ cell type classifications are representative of the known
181 timeline of the developing testis (**Figure 1B**), with only spermatogonia present at PND6,
182 some early spermatocytes present at PND14, much greater representation of those
183 spermatocytes at PND18, and appearance of more differentiated round and elongated
184 spermatids from PND25 onwards. Interestingly, we observed the greatest enrichment of
185 spermatids in the positively THY1-sorted adult sample, likely due to non-specific binding
186 of the antibody to the developing acrosome. Despite this, the library contained strong
187 representation of spermatogonia and spermatocytes and was therefore retained in the
188 analysis. The negative ACRV1 sorting for the other adult sample retained
189 representation of all germ cell types in the adult testis, including spermatogonia, which
190 would otherwise have been poorly represented due to the much greater abundance of
191 more differentiated cell types. Overall, both adult samples provide excellent
192 representation for all germ cell types present in the adult testis and are therefore
193 included in this sampling analysis.
194 Cell-free RNA contamination from lysed cells is a well-known confounding
195 feature in single-cell sequencing libraries, as highly-expressed transcripts from even a
196 small number of lysed cells can become incorporated in the gel bead emulsions of
197 single-cell microfluidics devices[18]. As a result of the incorporation of these transcripts
198 into libraries of cells from which they did not originate, cells which do not endogenously
199 express such transcripts can appear to have low levels of expression of these markers.
200 In this data set, genes highly expressed in elongated spermatids/sperm were detected
201 at low levels in cells identified as spermatogonia and spermatocytes exclusively in
202 libraries made from testes aged 25 days or older (data not shown), the only samples in

203 which spermatids are present. Therefore, we believe the detection of these transcripts
204 in both spermatogonia and spermatocytes of older mice is due to contamination from
205 cell-free RNA derived from lysed spermatids. To mitigate the age-related biases this
206 signal might pose in down-stream analysis, markers of the spermatid/sperm population
207 (genes with a greater than 20:1 ratio of expression between spermatids and other germ
208 cell types), such as *Prm1/2*, have been filtered from the data set (**Table S2**).
209

210 **Spermatogonia display characteristic transcriptional signatures, but also novel**
211 **gene expression dynamics, over developmental age**

212 To better understand the developmental transitions that spermatogonia undergo
213 with age, genes variably-expressed with age were identified by Model-based Analysis of
214 Single Cell Transcriptomics (MAST)[19] (**Table S3**) and visualized as a heatmap (**Figure**
215 **4**). As spermatogonia become proportionally rarer with age (and therefore later-aged
216 individual libraries experience low representation), spermatogonia from libraries PND18,
217 PND25, and PND30 were merged with each other, as were spermatogonia from the two
218 adult samples. While marker genes, indicated in the top row, remain quite constant over
219 time, clear and novel differences can be observed in spermatogonial gene expression
220 over time, particularly in spermatogonia derived from PND6 testes. Several genes,
221 including those noted to the side of the heatmap, are observed to have robust
222 differential expression over time, and may play a role in the establishment and growth of
223 this spermatogonial pool which will support lifelong spermatogenesis.

224 In addition to MAST analysis for variable expression, Gene Set Enrichment
225 Analysis (GSEA) Time Series analysis[20] of Reactome pathways revealed differentially-

226 utilized pathways, which were then visualized using Enrichment Map in Cytoscape[21,22].
227 GSEA of variably-expressed genes in spermatogonia from mice of different ages
228 reveals significant changes in many pathways, including increasing expression of genes
229 related to RNA destabilization and protein degradation as well as WNT signaling, and
230 decreasing expression of genes related to asparagine metabolism, various signaling
231 pathways including TGFB, FGFR, and KIT, and transcriptional regulation (**Figure 5**
232 **&S6A, Table S4**). In particular, many critical signaling receptors and ligands, including
233 *Kit* and *KitL*[23–26], as well as *Fgf8* and *Fgfr1*[27,28], exhibit downregulation in spermatogonia
234 derived from mice of increasing age, consistent with overall altered paracrine signaling
235 around the basement membrane of the seminiferous tubules during testis maturation.
236

237 **Spermatocytes from the first wave of spermatogenesis are transcriptionally**
238 **distinct from steady-state spermatocytes**

239 It has been well established that meiotic regulation is distinct in the first wave of
240 meiosis from that of subsequent waves[6,14,15]. Thus, we sought to explain this
241 phenomenon in terms of the transcriptome profile of spermatocytes at discrete
242 developmental time points. Spermatocytes from the first meiotic wave compared to
243 steady-state (adult) ages were also subjected to MAST analysis, as described above
244 (**Figure 6**, **Table S5**). For this analysis, spermatocytes were abundant enough from all
245 libraries that each time point could be considered separately, except for PND6 in which
246 spermatocytes are not yet present. Notably, spermatocytes from PND14, which are only
247 just beginning Prophase I, demonstrate very distinct gene expression patterns from
248 spermatocytes at later time points and are not representative of the full spectrum of

249 meiotic cell types. Some genes, including those noted to the side of the heatmap, show
250 robust differential expression with age, highlighting differences between spermatocytes
251 derived from the first-wave (PND18) in contrast those which are derived from a self-
252 renewing SSC population (adult). Therefore, these genes were chosen for further
253 analysis and orthogonal validation.

254 GSEA time series analysis of Reactome pathway enrichment of variably
255 expressed genes in spermatocytes also reveals intriguing differentially utilized
256 pathways. From this analysis, we observe decreasing expression of genes related to
257 translation and post-transcriptional regulation, and increasing expression of genes
258 related to DNA replication, double strand break repair, and cell cycle regulation (**Figure**
259 **7 & S6B, Table S6**). Most notable in the list of genes upregulated in spermatocytes of
260 increasing age are those known to be essential to DNA repair, meiotic progression, and
261 crossover formation including *Brip1*[29], *Brca1* and *Brca2*[30–32], *Rad51*[33], *H2afx*[34] and
262 *Atm*[35]. Many of these pathways, particularly those related to double strand break repair
263 (which initiates meiotic recombination), may be crucial for understanding the molecular
264 mechanisms underlying fundamental differences in first-wave spermatocytes.
265

266 **Validation of differentially expressed genes demonstrates dynamic protein**
267 **expression within a defined cell type during testis maturation**

268 Candidate genes of interest (GOIs) identified in the single-cell sequencing data
269 were investigated using immunofluorescence, which allowed us to validate changes in
270 protein expression in the context of the native testis tissue. We used paraffin-embedded
271 testis tissue sections at postnatal ages PND 7, PND 13, PND 22, and 8 weeks of age to

272 characterize the same range of postnatal testis development as was captured in the
273 single-cell RNAseq data set. GOIs were selected by meeting several criteria including:
274 representation across several biological pathways, significantly differential expression in
275 a given cell type between mice of different ages, and availability of a commercial
276 immunofluorescence-verified and mouse-reactive antibody. For all validation of
277 spermatogonial candidates, double-staining was performed with an antibody against
278 'Promyelocytic Leukemia Zinc Finger Protein' (PLZF; aka ZBTB16), a well-characterized
279 marker of undifferentiated spermatogonia[36–38]. For all validation of spermatocyte
280 candidates, double-staining was performed with an antibody against 'Synaptonemal
281 Complex Protein 3' (SYCP3), to allow for visualization and staging of Prophase I-staged
282 cells[13,39]. SYCP3 marks the nuclei of spermatocytes through leptotene, zygotene,
283 pachytene, and diplotene stages of prophase I.

284 To profile a range of biological functions including metabolism, enzyme
285 'Asparaginase-Like 1' (ASRGL1; aka ALP1) was chosen for immunofluorescence
286 analysis. ASRGL1 is known to catalyze the hydrolysis of L-asparagine[40] and to clear
287 protein-damaging isoaspartyl-peptides[41], and while largely uncharacterized in the
288 mouse, has been found to be highly expressed in the human cervix, fallopian tube,
289 ovary, and testis[42]. Interestingly, ASRGL1 has been identified as a biomarker of
290 endometrial cancer[42–45], as well as an antigen in rodent sperm[46]. In the single-cell
291 sequencing dataset, *Asrgl1* was observed to be highly expressed in spermatogonia
292 from PND6 mice, with decreasing expression in this cell type of older mice (**Figure 4**).
293 Interestingly, *Asrgl1* was also shown to have dynamic expression in spermatocytes, with
294 the lowest expression detected in PND14 spermatocytes and increasing expression in

295 spermatocytes of older mice (**Figure 6, Table S5**). These results at the mRNA level
296 were corroborated by immunofluorescence data showing high expression of ASRGL1
297 protein in PND7 PLZF+ spermatogonia, with decreasing expression of the protein in
298 PND22 and adult PLZF+ spermatogonia (**Figure 8A, S7**). Furthermore, PND13 first-
299 wave pachytene spermatocytes express little ASRGL1 protein, with expression
300 becoming abundant in pachytene spermatocytes from PND22 and adult testes (**Figure**
301 **8B, S8**).

302 Significant differences in RNA stability and processing genes were also observed
303 in spermatogonia during postnatal testis development, with down-regulation of related
304 pathways over time. The RNA binding protein, 'RNA Binding Motif Protein, X-linked-like
305 2' (RBMXL2; aka HNRNPG-T) is a putative RNA regulator and splicing factor highly
306 expressed in the mouse testis, specifically in germ cells[47], with critical functions in
307 spermatogenesis[48]. Furthermore, disruptions in RBMXL2 expression and localization in
308 human testes are associated with azoospermia in men[49]. In the single-cell data set,
309 *Rbmx2* mRNA was observed to be highly expressed in spermatogonia from the
310 youngest mice, then decreasing with age, as well as expressed in all spermatocytes of
311 all ages (**Figure 4, Table S3**). Immunofluorescence of RBMXL2 protein demonstrates
312 high expression of the protein in all germ cells, including spermatogonia and
313 spermatocytes. Close inspection, however, reveals relatively higher expression of
314 RBMXL2 in PND7 PLZF+ spermatogonia compared to later time points, despite the
315 relatively consistent expression of RBMXL2 protein in all other germ cell stages at all
316 mouse ages (**Figure S9**).

317 ‘Double-sex and Mab-3 Related Transcription Factor B1’ (DMRTB1; aka DMRT6)
318 is a transcriptional regulator known to coordinate the developmental transition from
319 spermatogonial differentiation to meiotic entry[50]. As has been previously observed,
320 *Dmrtb1* mRNA is highly expressed in spermatogonia and early spermatocytes (**Figures**
321 **4 & 6**), which we have confirmed at the protein level by immunofluorescence. At
322 PND13, first-wave early leptotene spermatocytes, evidenced by spotty SYCP3, exhibit
323 nuclear DMRTB1 staining, while pachytene spermatocytes from all mouse ages lose
324 DMRTB1 expression. Interestingly, the nuclear staining in leptotene spermatocytes is
325 only observed at the earliest time point, PND13, and not seen in early Prophase I
326 spermatocytes of later spermatogenic waves (**Figure 9, S10**).
327 Finally, DNA damage response proteins ‘RAD51 Recombinase’ (RAD51) and
328 ‘Ataxia Telangiectasia Mutated’ (ATM) were profiled across spermatocytes from mice of
329 increasing age, as these represent particularly interesting candidate proteins whose
330 differential expression may be crucial to understanding aberrant recombination rates
331 and chromosome segregation in the first wave. Intriguingly, both RAD51 and ATM show
332 subtly, but decidedly, decreased expression in first-wave pachytene spermatocytes,
333 with increasing expression as mice age (**Figures 10, S11, S12**), as predicted from our
334 scRNAseq data. These observations of altered RAD51 staining intensity are consistent
335 with previous reports of significantly fewer RAD51 foci along chromosome cores of
336 juvenile C57bl/6 spermatocytes compared to those at 12 weeks of age[14]. Our RAD51
337 observations demonstrate overall decreased protein expression in the nucleus of
338 pachytene first-wave spermatocytes, with increasing expression by 3 weeks of age
339 (**Figure 10B, S12**). A similar dynamic is observed for ATM, which has robust

340 cytoplasmic staining as well as diffuse nuclear staining in pachytene spermatocytes[51].
341 Our data demonstrate decreased expression of ATM in both cellular compartments in
342 the first-wave spermatocytes, with increasing expression, particularly in the cytoplasm
343 of these cells, by 3 weeks of age (**Figure 10A, S11**). These age-dependent dynamics of
344 critical DNA damage response regulators are likely to contribute to the health and
345 viability of resulting spermatocytes and spermatozoa from these spermatogenic cycles,
346 and may underlie some of the functional differences observed in the first wave of
347 spermatogenesis.

348 Overall, these gene expression dynamics discovered from single-cell mRNA
349 sequencing are reproducible at the level of protein expression in the context of the
350 native tissue, and likely represent important development transitions both in
351 spermatogonia and spermatocytes. These data will be indispensable to investigate how
352 gene expression dynamics help to regulate the many critical developmental events,
353 including spermatogonial differentiation and meiotic progression, occurring in the
354 developing mouse testis.

355

356 ***Discussion***

357 We have performed the first comprehensive sampling and screening of mouse
358 germ cells from neonatal life through adulthood, to obtain transcriptional profiles at a
359 high, single-cell resolution. With the exception of the adult samples, which were sorted
360 to exclude the over-riding sperm component, all libraries were generated from single-
361 cell suspensions of all testicular cells. Adult samples were minimally processed with a
362 single-step magnetic cell sort to provide representation of all germ cell types in the adult

363 testis. Previously, single-cell-sequencing studies on sorted cells have provided valuable
364 information about specific, and marker-defined cell types. The study presented here,
365 however, focuses on profiling the germline during postnatal testis maturation,
366 importantly capturing the first-wave of spermatogonia and spermatocytes which exhibit
367 differences from later, steady-state spermatogenesis. Because of the progression of
368 ages profiled, we have captured changes in gene expression at single-cell resolution to
369 compare the developmental progression of spermatogenesis as mice age.

370 Germ cells subtypes in the testis are frequently defined by the presence or
371 absence of particular protein markers, which can be visualized by reporter expression or
372 immunofluorescence, or which can sometimes be used for flow cytometry or other
373 enrichment paradigms. Spermatogonia are often defined as cells which express a key
374 complement of protein markers, such as PLZF or 'GDNF family receptor alpha 1'
375 (GFRα1)[52–54]. While this is the best practice for visual identification of cells for which
376 discrete markers have been elusive, such as spermatogonia, our analysis suggests that
377 the biology of these cells during postnatal testis development is far more complicated
378 that previously understood. Our analysis stresses that defining these cell populations on
379 the basis of specific markers may be overly simplistic, despite being the current
380 standard practice in the field. Primary spermatocytes are similarly distinct at the
381 transcriptional level over developmental time. Furthermore, cells possessing an SYCP3-
382 positive synaptonemal complex indicative of pachynema also exhibit differences in
383 immunolocalized proteins during testis maturation, indicating that they, too, exhibit
384 distinct and variable translational dynamics with increasing age. Critically, this analysis
385 reveals that, while known markers may be useful for defining primary cell identity, there

386 are many changes in spermatogenesis that have been under-appreciated without the
387 power of single-cell resolution of gene expression profiling.

388 Specifically, we show here that PLZF-defined spermatogonia, though retaining
389 PLZF-positivity, are transcriptionally distinct at PND6 compared to later developmental
390 time points. These transcriptional dynamics are also reflected by distinct differences at
391 the protein level, with proteins such ASRGL1 being localized strongly in PLZF+
392 spermatogonia during the first weeks of life, but decreasing in expression in these cells
393 around three weeks of age (**Figure 8A, S7**). Similarly, we show that Prophase I
394 spermatocytes possess significant transcriptional differences in the first-wave compared
395 to subsequent spermatogenic waves, with hundreds of differentially expressed genes
396 across multiple regulatory pathways. Furthermore, direct inspection of pachytene
397 spermatocytes from the first wave at PND13 to later spermatogenic waves reveals that,
398 like spermatogonia, transcript dynamics are also reflected at the protein level. For
399 example, proteins such as DMRTB1 are found only in the nuclei of first-wave leptotene
400 spermatocytes as they transition from differentiated spermatogonia into the meiotic
401 program, but not in spermatocytes from older mice (**Figure 9, S10**). By contrast, other
402 proteins such as ASRGL1 are in low abundance in early first-wave spermatocytes, but
403 become more strongly immunolocalized in spermatocytes at increasing ages (**Figure**
404 **8B, S8**).

405 In addition to the transcriptional and translational dynamics in defined cell types
406 over time, these data also reveal differential utilization of particular biological pathways
407 over developmental time. Gene set enrichment analysis[20] utilizing the Reactome
408 pathway database[21,22] has demonstrated that spermatogonia dramatically change their

transcriptional landscape as mice age, including downregulation of genes within essential meiotic-entry-associated SCF/KIT[26,55] and FGFR[56] pathways, including *Kit* and *KitL*. While we cannot rule out the possibility that variable gene expression in spermatogonia is, in part, due to differential contributions of the spermatogonial stem cell population at different ages – with decreasing contribution as mice age – this dataset provides strong support for true variable gene expression in the spermatogonial pool. For instance, while spermatogonia derived from older mice exhibit downregulation of genes associated with FGFR signaling, including *Fgf8* and *Fgfr1*, and could indicate decreased representation of an undifferentiated spermatogonial population[28], this is in opposition to observed coincident decreased expression of *Kit* and *KitL* which would support increased representation of an undifferentiated population[24,26,55]. Therefore, these data likely reflect overall changes to the paracrine signaling of the spermatogonial stem cell niche as well as the basement membrane as mice age. Overall, these data suggest spermatogonia may modulate their sensitivity for particular critical signaling pathways, which may affect their competency to commit to the meiotic program. Furthermore, pathways associated with mRNA stability and protein degradation are upregulated as the testis matures, suggesting that spermatogonia from older mice may change their capacity for post-transcriptional and post-translational regulation with age, possibly reflecting changing demands for growth and proliferation in older animals.

Similar to spermatogonia, spermatocytes also exhibit differential utilization of specific biological pathways with age, an observation that dovetails with the knowledge that spermatocytes derived from the first wave of spermatogenesis are functionally different to those spermatocytes derived from steady-state spermatogenesis. First-wave

432 spermatocytes are known to exhibit several unique, and some detrimental,
433 characteristics, including reduced recombination rate[14,15] and greater incidence of
434 chromosome mis-segregation[15]. These features result in first-wave spermatozoa which
435 are often much less reproductively successful than those which will arise from the self-
436 renewing SSC population later in life[57,58]. Our data presented here demonstrate age-
437 related upregulation of pathways associated with DNA replication and repair, double
438 strand break repair, and response to DNA damage, all of which may underlie the well-
439 characterized differences between spermatocytes in the first wave compared to steady-
440 state spermatocytes. Included in these sets of variably-expressed genes are known
441 regulators of DNA damage response and cross-over formation including *Rad51*[33],
442 *Brip1*[29], *and H2afx*[34], as well as *Brca1* and *Brca2*[30–32] and *Atm*[35,59], all of which increase
443 in spermatocytes with age, effects which we have also shown at the protein level for
444 both RAD51 and ATM (**Figures 10, S11, S12**). While the cause of this lower expression
445 in the first wave is unknown, it has been demonstrated that spermatocytes from juvenile
446 mice generate only about 25% of the double strand breaks present in spermatocytes
447 from steady-state spermatogenesis[59]. It is possible that in response to fewer breaks,
448 less DNA damage response machinery is required and therefore exhibits lower
449 expression levels. Alternatively, these observations may also suggest that steady-state
450 spermatocytes acquire greater competency to cope with the DNA damage inherent to
451 meiotic progression, and that spermatocytes in the first wave may not execute these
452 pathways as successfully, resulting in the observed recombination differences and
453 increased chromosome mis-segregation. Notably, like spermatogonia, spermatocytes
454 also experience alteration of pathways related to translation and mRNA stability,

455 emphasizing the myriad ways in which gene expression is regulated in developing germ
456 cells. Ultimately, this differential pathway utilization may help to explain not only the
457 functional differences observed in spermatocytes and spermatozoa from juveniles, but
458 may also improve our understanding of increased birth defects associated with young
459 paternal age[57,58].

460 Another of our primary objectives in undertaking this analysis was to potentially
461 reveal new markers of the spermatogonial stem cell population. Despite many efforts to
462 define this population by both cytoplasmic and nuclear markers, discrete markers of this
463 population have remained elusive and controversial [60–63]. Our data are supportive of the
464 high degree of heterogeneity of this cell population, not only within the population at a
465 single age, but also across ages. Furthermore, markers which have become accepted
466 in the field, such as expression of 'Inhibitor of DNA Binding 4' (*Id4*)[64–66], show
467 widespread detection in spermatogonia through spermatocytes, while markers such as
468 *Zbtb16* (*Plzf*) and *Gfrα1* have much more restricted expression (**Figure S5**).
469 Importantly, expression patterns of these popular markers are not entirely self-
470 consistent. It is therefore likely that the spermatogonial population is not discrete, but is
471 indeed a continuous or plastic population[67,68]. Despite this, these data remain a valuable
472 resource to those interested in understanding the molecular mechanisms underlying
473 SSC self-renewal and differentiation, though the biology may not be as simplistic as
474 originally thought.

475 Taken together, these data represent the first comprehensive sampling and
476 profiling of spermatogonia and spermatocytes during development of the mouse testis.
477 These data emphasize the necessity of considering not only the protein markers for

478 which individual cells are positive, but also the age of the cells being analyzed. These
479 observations of highly dynamic gene expression in germ cell populations during
480 postnatal testis development stress that germ cells of a particular age or identity
481 possess vastly different underlying biology and that consideration must be given to
482 these dynamics when profiling germ cell populations. These data also represent an
483 invaluable community resource for discovery of previously unknown gene expression
484 dynamics and pathway contributions that may be critical for the many developmental
485 transitions in the male germ cell population which are essential for successful
486 spermatogenesis and fertility.
487

488 ***Methods***

489 **Animals**

490 B6D2F1/J mice were generated by mating C57bl/6 female mice with DBA/2J
491 male mice. All animal protocols were reviewed and approved by the Cornell University
492 Institutional Animal Care and Use Committee and were performed in accordance with
493 the National Institutes of Health Guide for the Care and Use of Laboratory Animals.
494 Mice were maintained on standard light:dark cycles with laboratory mouse chow
495 provided *ad libidum.*
496

497 **Generation of testis single cell libraries**

498 Testes were collected from mice (n = 1 mouse, 2 testes for each time point) at
499 postnatal (PND) days 6, 14, 18, 25, 30, and 8 weeks of age, and dissociated per
500 standard protocols for germ cell enrichment[16]. Briefly, testes were held in 1X HBSS

501 buffer before de-tunicating and moving tubules into 0.25% Trypsin. Tubules were further
502 dissociated by trituration and addition of DNase to a final concentration of 7 mg/ml.
503 Tubules were placed in a 37°C incubation for 5 minutes at a time, and then removed for
504 further trituration. Incubations at 37°C were performed three times, until a cloudy
505 suspension was achieved. Cells were passed through a 40 μM filter, spun down, and re-
506 suspended in 10ml 1X Dulbecco's PBS + 10% Knockout Serum Replacement (DPBS-
507 S). This cell suspension was then layered on top of a 30% Percoll solution. Cells were
508 then spun down again, and the resulting pellet was re-suspended in 1ml DPBS-S. As a
509 technical control, cells from PND18 were split into two samples after the 40 μM filter,
510 with one half of the cells processed with the Percoll gradient, and the other half directly
511 re-suspended in its final buffer with no Percoll sedimentation, resulting in libraries
512 "PND18" and "PND18pre", respectively. Due to the similarities between these libraries
513 (**Figure S1**), the data from these libraries were thereafter combined and analyzed
514 together as "PND18".

515 For adult testes only, the resulting cell suspension was split in half and sorted
516 with magnetic beads in two ways: (1) sperm-depletion was performed by incubating the
517 cells for 30 minutes with 20 μl anti-ACRV1-PE (Novus Biologicals #NB500-455PE),
518 washing with DPBS-S, incubating the cells for 30 minutes with 20 μl magnetic-bead-
519 conjugated anti-PE (Miltenyi Biotec #130-048-801), and finally performing a negative
520 magnetic selection. Cells were applied to a Miltenyi Biotec MACS LS column, and flow-
521 through cells were collected, as sperm were to remain bound to the ferromagnetic
522 column. (2) THY1+ spermatogonia were enriched by incubating the cells for 60 minutes
523 with 20 μl magnetic-bead-conjugated anti-CD90.2 (THY1) (Miltenyi Biotec #130-102-

524 464), and finally performing a positive magnetic selection. Cells were applied to the
525 column, flow-through cells were discarded, and antibody-bound cells were eluted from
526 the ferromagnetic column. These cells were then spun down and re-suspended in 1ml
527 DPBS-S as above.

528 The resulting cells from all samples were submitted to the Cornell DNA
529 Sequencing Core Facility for processing on the 10X Genomics Chromium System with a
530 target of 4-5000 cells per sample. Sequencing libraries were generated using the 10X
531 Genomics Chromium Single Cell 3′ RNAseq v2 kit, tested for quality control on an ABI
532 DNA Fragment Analyzer, and run on a NextSeq platform with 150 base-pair reads.
533 Libraries were sequenced to average depth 98M reads (range 77M-124M); on average,
534 91% of reads (range 89%-92%) mapped to the reference genome.
535

536 **Single-cell transcriptome analysis**

537 Data normalization, unsupervised cell clustering, and differential expression were
538 carried out using the Seurat R package[69]. Batch effect and cell-cycle effect were
539 removed by Combat[70] and Seurat together. Cells with less than 500 genes or 2000
540 UMIs or more than 15% of mitochondria genes were excluded from the analysis. Gene
541 expression raw counts were normalized following a global-scaling normalization method
542 with a scale factor of 10,000 and a log2 transformation, using the Seurat NormalizeData
543 function. The top 4000 highly variable genes were selected using the expression and
544 dispersion (variance/mean) of genes. Combat removed batch effects. Seurat regressed
545 the difference between the G2M and S phase, then followed by principal component
546 analysis (PCA). The most significant principal components (1-30) were used for

547 unsupervised clustering and t-Distributed Stochastic Neighbor Embedding (tSNE)
548 analysis.
549 Cell types were manually identified by marker genes[71–73], and confirmed by
550 SingleR (Single-cell Recognition) package. Differential expression analysis was
551 performed based on the MAST (Model-based Analysis of Single Cell Transcriptomics)[19].
552 Gene Set Enrichment Time Series Analysis[20] used the differential expression based on
553 each time point, after removing genes highly expressed in spermatids. Pathways were
554 visualized by EnrichmentMap[22] in Cytoscape[21].
555 Code availability: The scripts used for analysis and figure generation are
556 available at https://github.com/nyuhuyang/scRNAseq-SSCs
557 Data availability: The single-cell RNAseq data have been deposited at GEO and
558 are accessible through Series accession number: GSE121904.
559
560 **Immunofluorescence validation**
561 Testes were collected, cleaned of excess fat, and fixed in 0.1% formalin solution
562 overnight before dehydration and embedding in paraffin. Fixed testes were sectioned at
563 5 μm onto glass slides by the Cornell Animal Health Diagnostic Center. To stain,
564 sections were de-paraffinized by 3x, 5 minute washes in Histoclear followed by
565 rehydration in 100% ethanol (2x, 5 minutes), 95% ethanol (2x, 5 minutes), 70% ethanol
566 (1x, 5 minutes), water (1x, 5minutes). Sections were then incubated in boiling antigen
567 retrieval buffer (10 mM sodium citrate, 0.05% Tween-20, pH 6.0) for 20 minutes and left
568 to cool. Sections were washed 3x, 5 minutes in 1X PBS + 0.1% Triton-X (PBST). Tissue
569 sections were then incubated in blocking buffer [3% Goat Serum (Sigma), 1% Bovine

570 Serum Albumin (Sigma), and 0.5% Triton-X (Fisher Scientific) in 1X PBS] and stained
571 by incubation with primary antibodies against PLZF, SYCP3, RBMXL2, ASRGL1,
572 DMRTB1, RAD51, and ATM (see **Table S7**) overnight at 4°C. The following day, slides
573 were washed 3x, 5 minutes in PBST and then incubated with secondary antibodies
574 raised in goat against mouse (594 nm) and rabbit (488 nm) at 1:500 for 1 hour at 37°C.
575 A secondary antibody-only control was included to assess background staining.
576 Sections were further stained with DAPI to visualize nuclei, mounted and analyzed on
577 an Epifluorescent Zeiss Axioplan microscope. For all time points for a given set of
578 antibodies, images were exposed equivalently.
579
580
581
582
583
584
585
586
587
588
589
590
591
592

593 **References**

594 1. Phillips, B. T., Gassei, K. & Orwig, K. E. Spermatogonial stem cell regulation and
595 spermatogenesis. *Philos. Trans. R. Soc. Lond. B. Biol. Sci.* **365,** 1663–78 (2010).
596 2. Lawson, K. A. & Hage, W. J. *Germline development*. *Ciba Foundation*
597 *Symposium* **182,** (Wiley, 1994).
598 3. Anderson, R., Copeland, T. K., Schöler, H., Heasman, J. & Wylie, C. The onset of
599 germ cell migration in the mouse embryo. *Mech. Dev.* **91,** 61–68 (2000).
600 4. Nakatsuji, N. & Chuma, S. Differentiation of mouse primordial germ cells into
601 female or male germ cells. *Int. J. Dev. Biol.* **45,** 541–8 (2001).
602 5. Ewen, K. A. & Koopman, P. Mouse germ cell development: From specification to
603 sex determination. *Molecular and Cellular Endocrinology* **323,** 76–93 (2010).
604 6. Yoshida, S. *et al.* The first round of mouse spermatogenesis is a distinctive
605 program that lacks the self-renewing spermatogonia stage. *Development* **133,**
606 1495–1505 (2006).
607 7. Tegelenbosch, R. & de Rooij, D. A quantitative study of spermatogonial
608 multiplication and stem cell renewal in the C3H/101 F1 hybrid mouse. *Mutat. Res.*
609 **290,** 193–200 (1993).
610 8. Koubova, J. *et al.* Retinoic acid regulates sex-specific timing of meiotic initiation in
611 mice. *Proc. Natl. Acad. Sci.* **103,** 2474–2479 (2006).
612 9. Anderson, E. L. *et al.* Stra8 and its inducer, retinoic acid, regulate meiotic initiation
613 in both spermatogenesis and oogenesis in mice. *Proc. Natl. Acad. Sci. U. S. A.*
614 **105,** 14976–14980 (2008).
615 10. Endo, T. *et al.* Periodic retinoic acid–STRA8 signaling intersects with periodic

616 germ-cell competencies to regulate spermatogenesis. *Proc. Natl. Acad. Sci.* **112,**
617 E2347–E2356 (2015).
618 11. Endo, T., Freinkman, E., de Rooij, D. G. & Page, D. C. Periodic production of
619 retinoic acid by meiotic and somatic cells coordinates four transitions in mouse
620 spermatogenesis. *Proc. Natl. Acad. Sci.* **114,** E10132–E10141 (2017).
621 12. Baarends, W. M. *et al.* Chromatin dynamics in the male meiotic prophase.
622 *Cytogenet. Genome Res.* **103,** 225–34 (2003).
623 13. Gray, S. & Cohen, P. E. Control of Meiotic Crossovers: From Double-Strand
624 Break Formation to Designation. *Annu. Rev. Genet.* **50,** 175–210 (2016).
625 14. Vrooman, L. A., Nagaoka, S. I., Hassold, T. J. & Hunt, P. A. Evidence for paternal
626 age-related alterations in meiotic chromosome dynamics in the mouse. *Genetics*
627 **196,** 385–96 (2014).
628 15. Zelazowski, M. J., Sandoval, M. & Gribbell, M. A. Age-Dependent Alterations in
629 Meiotic Recombination Cause Chromosome Segregation Errors in Spermatocytes
630 In Brief. *Cell* **171,** 601–607.e13 (2017).
631 16. Goodyear, S. & Brinster, R. Isolation of the Spermatogonial Stem Cell-Containing
632 Fraction from Testes. *Cold Spring Harb. Protoc.* **2017,** pdb.prot094185 (2017).
633 17. Osuru, H. P. *et al.* The acrosomal protein SP-10 (*Acrv1*) is an ideal marker for
634 staging of the cycle of seminiferous epithelium in the mouse. *Mol. Reprod. Dev.*
635 **81,** 896–907 (2014).
636 18. Zheng, G. X. Y. *et al.* Massively parallel digital transcriptional profiling of single
637 cells. *Nat. Commun.* **8,** 14049 (2017).
638 19. Finak, G. *et al.* MAST: a flexible statistical framework for assessing transcriptional

639 changes and characterizing heterogeneity in single-cell RNA sequencing data.
640 *Genome Biol.* **16,** 278 (2015).
641 20. Subramanian, A. *et al.* Gene set enrichment analysis: a knowledge-based
642 approach for interpreting genome-wide expression profiles. *Proc. Natl. Acad. Sci.*
643 *U. S. A.* **102,** 15545–50 (2005).
644 21. Shannon, P. *et al.* Cytoscape: a software environment for integrated models of
645 biomolecular interaction networks. *Genome Res.* **13,** 2498–504 (2003).
646 22. Merico, D., Isserlin, R., Stueker, O., Emili, A. & Bader, G. D. Enrichment map: a
647 network-based method for gene-set enrichment visualization and interpretation.
648 *PLoS One* **5,** e13984 (2010).
649 23. Kubota, H., Avarbock, M. R. & Brinster, R. L. Spermatogonial stem cells share
650 some, but not all, phenotypic and functional characteristics with other stem cells.
651 *Proc. Natl. Acad. Sci.* **100,** 6487–6492 (2003).
652 24. Schrans-Stassen, B. H. G. J., van de Kant, H. J. G., de Rooij, D. G. & van Pelt, A.
653 M. M. Differential Expression of c- *kit* in Mouse Undifferentiated and
654 Differentiating Type A Spermatogonia. *Endocrinology* **140,** 5894–5900 (1999).
655 25. Busada, J. T., Niedenberger, B. A., Velte, E. K., Keiper, B. D. & Geyer, C. B.
656 Mammalian target of rapamycin complex 1 (mTORC1) Is required for mouse
657 spermatogonial differentiation in vivo. *Dev. Biol.* **407,** 90–102 (2015).
658 26. Vincent, S. *et al.* Stage-specific expression of the Kit receptor and its ligand (KL)
659 during male gametogenesis in the mouse: a Kit-KL interaction critical for meiosis.
660 *Development* **125,** 4585–93 (1998).
661 27. Pui, H. P. & Saga, Y. Gonocytes-to-spermatogonia transition initiates prior to birth

662 in murine testes and it requires FGF signaling. *Mech. Dev.* **144,** 125–139 (2017).
663 28. Hasegawa, K. & Saga, Y. FGF8-FGFR1 Signaling Acts as a Niche Factor for
664 Maintaining Undifferentiated Spermatogonia in the Mouse1. *Biol. Reprod.* **91,** 145
665 (2014).
666 29. Sun, X. *et al.* FancJ (Brip1) loss-of-function allele results in spermatogonial cell
667 depletion during embryogenesis and altered processing of crossover sites during
668 meiotic prophase I in mice. *Chromosoma* **125,** 237–52 (2016).
669 30. Blackshear, P. E. *et al.* Brca1 and Brca2 expression patterns in mitotic and
670 meiotic cells of mice. *Oncogene* **16,** 61–68 (1998).
671 31. Simhadri, S. *et al.* Male fertility defect associated with disrupted BRCA1-PALB2
672 interaction in mice. *J. Biol. Chem.* **289,** 24617–29 (2014).
673 32. Broering, T. J. *et al.* BRCA1 establishes DNA damage signaling and pericentric
674 heterochromatin of the X chromosome in male meiosis. *J. Cell Biol.* **205,** 663–75
675 (2014).
676 33. Haaf, T., Golub, E. I., Reddy, G., Radding, C. M. & Ward, D. C. Nuclear foci of
677 mammalian Rad51 recombination protein in somatic cells after DNA damage and
678 its localization in synaptonemal complexes. *Proc. Natl. Acad. Sci. U. S. A.* **92,**
679 2298–302 (1995).
680 34. Testa, E. *et al.* H2AFX and MDC1 promote maintenance of genomic integrity in
681 male germ cells. *J. Cell Sci.* **131,** jcs214411 (2018).
682 35. Plug, A. W. *et al.* ATM and RPA in meiotic chromosome synapsis and
683 recombination. *Nat. Genet.* **17,** 457–461 (1997).
684 36. Costoya, J. A. *et al.* Essential role of Plzf in maintenance of spermatogonial stem

685 cells. *Nat. Genet.* **36,** 653–659 (2004).
686 37. Filipponi, D. *et al.* Repression of kit Expression by Plzf in Germ Cells. *Mol. Cell.*
687 *Biol.* **27,** 6770–6781 (2007).
688 38. Lovelace, D. L. *et al.* The regulatory repertoire of PLZF and SALL4 in
689 undifferentiated spermatogonia. *Development* **143,** 1893–1906 (2016).
690 39. Yuan, L. *et al.* The murine SCP3 gene is required for synaptonemal complex
691 assembly, chromosome synapsis, and male fertility. *Mol. Cell* **5,** 73–83 (2000).
692 40. Cantor, J. R., Stone, E. M., Chantranupong, L. & Georgiou, G. The Human
693 Asparaginase-like Protein 1 hASRGL1 Is an Ntn Hydrolase with β-Aspartyl
694 Peptidase Activity. *Biochemistry* **48,** 11026–11031 (2009).
695 41. Biswas, P. *et al.* A missense mutation in *ASRGL1* is involved in causing
696 autosomal recessive retinal degeneration. *Hum. Mol. Genet.* **25,** ddw113 (2016).
697 42. Edqvist, P.-H. D. *et al.* Loss of ASRGL1 expression is an independent biomarker
698 for disease-specific survival in endometrioid endometrial carcinoma. *Gynecol.*
699 *Oncol.* **137,** 529–537 (2015).
700 43. Fonnes, T. *et al.* Asparaginase-like protein 1 expression in curettage
701 independently predicts lymph node metastasis in endometrial carcinoma: a
702 multicenter study. *BJOG An Int. J. Obstet. Gynaecol.* (2018). doi:10.1111/1471-
703 0528.15403
704 44. Huvila, J. *et al.* Combined ASRGL1 and p53 immunohistochemistry as an
705 independent predictor of survival in endometrioid endometrial carcinoma.
706 *Gynecol. Oncol.* **149,** 173–180 (2018).
707 45. Fonnes, T. *et al.* Asparaginase-like protein 1 is an independent prognostic marker

708 in primary endometrial cancer, and is frequently lost in metastatic lesions.
709 *Gynecol. Oncol.* **148,** 197–203 (2018).
710 46. Bush, L. A. *et al.* A novel asparaginase-like protein is a sperm autoantigen in rats.
711 *Mol. Reprod. Dev.* **62,** 233–247 (2002).
712 47. Elliott, D. J. *et al.* An evolutionarily conserved germ cell-specific hnRNP is
713 encoded by a retrotransposed gene. *Hum. Mol. Genet.* **9,** 2117–2124 (2000).
714 48. Ehrmann, I. *et al.* Haploinsufficiency of the germ cell-specific nuclear RNA binding
715 protein hnRNP G-T prevents functional spermatogenesis in the mouse. *Hum. Mol.*
716 *Genet.* **17,** 2803–2818 (2008).
717 49. Maymon, B. B.-S. *et al.* Localization of the germ cell-specific protein, hnRNP G-T,
718 in testicular biopsies of azoospermic men. *Acta Histochem.* **104,** 255–261 (2002).
719 50. Zhang, T., Murphy, M. W., Gearhart, M. D., Bardwell, V. J. & Zarkower, D. The
720 mammalian Doublesex homolog DMRT6 coordinates the transition between
721 mitotic and meiotic developmental programs during spermatogenesis.
722 *Development* **141,** 3662–3671 (2014).
723 51. Hamer, G., Kal, H. B., Westphal, C. H., Ashley, T. & de Rooij, D. G. Ataxia
724 Telangiectasia Mutated Expression and Activation in the Testis1. *Biol. Reprod.*
725 **70,** 1206–1212 (2004).
726 52. Meng, X. *et al.* Regulation of cell fate decision of undifferentiated spermatogonia
727 by GDNF. *Science* **287,** 1489–93 (2000).
728 53. Hofmann, M.-C., Braydich-Stolle, L. & Dym, M. Isolation of male germ-line stem
729 cells; influence of GDNF. *Dev. Biol.* **279,** 114–124 (2005).
730 54. Kubota, H., Avarbock, M. R. & Brinster, R. L. Growth factors essential for self-

731 renewal and expansion of mouse spermatogonial stem cells. *Proc. Natl. Acad.*
732 *Sci.* **101,** 16489–16494 (2004).
733 55. Busada, J. T. *et al.* Retinoic acid regulates Kit translation during spermatogonial
734 differentiation in the mouse. *Dev. Biol.* **397,** 140–149 (2015).
735 56. Gonzalez-Herrera, I. G. *et al.* Testosterone regulates FGF-2 expression during
736 testis maturation by an IRES-dependent translational mechanism. *FASEB J.* **20,**
737 476–8 (2006).
738 57. Roecker, G. O. & Huether, C. A. An analysis for paternal-age effect in Ohio's
739 Down syndrome births, 1970-1980. *Am. J. Hum. Genet.* **35,** 1297–306 (1983).
740 58. Steiner, B. *et al.* An unexpected finding: younger fathers have a higher risk for
741 offspring with chromosomal aneuploidies. *Eur. J. Hum. Genet.* **23,** 466–72 (2015).
742 59. Lange, J. *et al.* ATM controls meiotic double-strand-break formation. *Nature* **479,**
743 237–240 (2011).
744 60. YOSHIDA, S., NABESHIMA, Y.-I. & NAKAGAWA, T. Stem Cell Heterogeneity:
745 Actual and Potential Stem Cell Compartments in Mouse Spermatogenesis. *Ann.*
746 *N. Y. Acad. Sci.* **1120,** 47–58 (2007).
747 61. Zheng, K., Wu, X., Kaestner, K. H. & Wang, P. The pluripotency factor LIN28
748 marks undifferentiated spermatogonia in mouse. *BMC Dev. Biol.* **9,** 38 (2009).
749 62. Hermann, B. P., Phillips, B. T. & Orwig, K. E. The Elusive Spermatogonial Stem
750 Cell Marker?1. *Biol. Reprod.* **85,** 221–223 (2011).
751 63. Gassei, K. & Orwig, K. E. SALL4 Expression in Gonocytes and Spermatogonial
752 Clones of Postnatal Mouse Testes. *PLoS One* **8,** e53976 (2013).
753 64. Sablitzky, F. *et al.* Stage- and subcellular-specific expression of Id proteins in

754 male germ and Sertoli cells implicates distinctive regulatory roles for Id proteins
755 during meiosis, spermatogenesis, and Sertoli cell function. *Cell Growth Differ.* **9,**
756 1015–24 (1998).
757 65. Oatley, M. J., Kaucher, A. V., Racicot, K. E. & Oatley, J. M. Inhibitor of DNA
758 Binding 4 Is Expressed Selectively by Single Spermatogonia in the Male Germline
759 and Regulates the Self-Renewal of Spermatogonial Stem Cells in Mice1. *Biol.*
760 *Reprod.* **85,** 347–356 (2011).
761 66. Sun, F., Xu, Q., Zhao, D. & Degui Chen, C. Id4 Marks Spermatogonial Stem Cells
762 in the Mouse Testis. *Sci. Rep.* **5,** 17594 (2015).
763 67. Morimoto, H. *et al.* Phenotypic Plasticity of Mouse Spermatogonial Stem Cells.
764 *PLoS One* **4,** e7909 (2009).
765 68. Cooke, P. S., Simon, L., Nanjappa, M. K., Medrano, T. I. & Berry, S. E. Plasticity
766 of spermatogonial stem cells. *Asian J. Androl.* **17,** 355–9
767 69. Butler, A., Hoffman, P., Smibert, P., Papalexi, E. & Satija, R. Integrating single-
768 cell transcriptomic data across different conditions, technologies, and species.
769 *Nat. Biotechnol.* **36,** 411–420 (2018).
770 70. Johnson, W. E., Li, C. & Rabinovic, A. Adjusting batch effects in microarray
771 expression data using empirical Bayes methods. *Biostatistics* **8,** 118–27 (2007).
772 71. Soumillon, M. *et al.* Cellular source and mechanisms of high transcriptome
773 complexity in the mammalian testis. *Cell Rep.* **3,** 2179–90 (2013).
774 72. Min Jung, Daniel Wells, Janette Rusch, Suhaira Ahmed, Jonathan Marchini,
775 Simon Myers, D. C. Unified single-cell analysis of testis gene regulation and
776 pathology in 5 mouse strains. *BioRxiv* (2018).

73. von Kopylow, K. & Spiess, A.-N. Human spermatogonial markers. *Stem Cell Res.* **25,** 300–309 (2017).

800 **Figure Legend**

801

802 **Figure 1** – *Germ cells profiled in single-cell sequencing analysis are representative of*
803 *known biology of the developing testis*. A) Schematic of the developing testis with germ
804 cell representation at each time point. Only spermatogonia are present during the first
805 week of life, until meiotic entry at PND10, after which germ cells can commit meiosis
806 and progress through spermatogenesis and spermiogenesis, producing the first mature
807 spermatozoa from the first wave around PND30. B) Germ cell composition by proportion
808 and absolute cell number from each library-of-origin.

809

810 **Figure 2** – *Clustering of single-cell data into libraries-of-origin and cell type*
811 *classifications.* A) tSNE representation of all cells with >500 detected genes and >2000
812 UMIs, color-coded by library-of-origin B) tSNE representation of all cells with >500
813 detected genes and >2000 UMIs, color-coded by cell type classification.

814

815 **Figure 3** – *Marker gene heatmap of all germ cell types reveals known signatures.*
816 Heatmap of most-differentially-expressed marker genes per germ cell type. Color bar at
817 the bottom indicates library-of-origin time point for cells within each block. Expression is
818 represented as a z-score ranging from -2 to 2. Notable marker genes for each germ cell
819 type are highlighted to the right of the heatmap. The adult sperm-depleted sample is
820 named “Ad S-D” while the adult THY1-sorted sample is named “Ad T-S”.

821

822 **Figure 4** – *Analysis of variably-expressed genes in spermatogonia*. MAST analysis was
823 used to determine genes which are variably expressed with age specifically in
824 spermatogonia, represented in a heatmap. All genes represented in the heatmap and
825 listed in Table S3 are differentially expressed with the exception of the marker genes
826 which remain consistently expressed. PND18-30 time points have been merged to
827 increase representation of this rare cell type at those time points. Similarly, adult time
828 points have also been merged. Individual cells are plotted vertically and the libraries
829 from which they are derived is indicated at the bottom of the heatmap. Individual genes
830 are plotted horizontally and the color bar at the left indicates library-of-origin from which
831 highest expression is observed. Expression is scaled, ranging from 0 to 2.5.
832
833 **Figure 5** – *Differential Reactome pathway utilization in spermatogonia with age.* Gene
834 set enrichment analysis of variably-expressed genes in the Reactome database was
835 visualized in Cytoscape. Results were filtered on a false discovery rate <0.05, and a
836 gene set list >45 genes. Red nodes indicate pathways upregulated with time while blue
837 nodes indicate pathways down-regulated with time. Edges indicate connections and
838 overlap between pathways.
839
840 **Figure 6** - *Analysis of variably-expressed genes in spermatocytes*. MAST analysis was
841 used to determine genes which are variably expressed with age specifically in
842 spermatocytes, represented in a heatmap. All genes represented in the heatmap and
843 listed in Table S5 are differentially expressed with the exception of the marker genes
844 which remain consistently expressed. Individual cells are plotted vertically and the

845 libraries from which they are derived is indicated at the bottom of the heatmap.
846 Individual genes are plotted horizontally and the color bar at the left indicates library-of-
847 origin from which the highest expression is observed. Expression is scaled, ranging
848 from 0 to 2.5. The adult sperm-depleted sample is named “Ad S-D” while the adult
849 THY1-sorted sample is named “Ad T-S”.
850
851 **Figure 7** - *Differential Reactome pathway utilization in spermatocytes with age.* Gene
852 set enrichment analysis of variably-expressed genes in the Reactome database was
853 visualized in Cytoscape. Results were filtered on a false discovery rate <0.05, and a
854 gene set list >15 genes. Red nodes indicate pathways upregulated with time while blue
855 nodes indicate pathways down-regulated with time. Edges indicate connections and
856 overlap between pathways. The tables to the left of the diagrams identify notable genes
857 represented in these pathways.
858
859 **Figure 8** – *ASRGL1 is highly expressed specifically in spermatogonia from neonatal*
860 *and juvenile mice, and spermatocytes of older mice.* A) Spermatogonial marker PLZF
861 (red) and ASRGL1 (green) were stained in 5μm testis tissue sections from mice ages
862 PND7, PND13, PND22, and adult. DAPI (blue) denotes nuclei. ASRGL1 protein
863 expression decreases in PLZF+ spermatogonia with age. B) Spermatocyte marker
864 SYCP3 (red) and ASRGL1 (green) were stained in 5μm testis tissue sections from mice
865 ages PND13, PND22, and adult. ASRGL1 protein expression increases in SYCP3+
866 spermatocytes with age. For all images, high-ASRGL1-expressing spermatogonia are

867 indicated by full arrows with a line, while low-ASRGL1-expressing spermatogonia are
868 indicated by arrowheads.
869
870 **Figure 9** – *DMRTB1 is highly expressed specifically in first-wave spermatocytes from*
871 *juvenile mice.* Spermatocyte marker SYCP3 (red) and DMRTB1 (green) were stained in
872 5μm testis tissue sections from mice ages PND13, PND22, and adult. DMRTB1 protein
873 is expressed in the nucleus of first-wave spermatocytes at PND13, with decreasing
874 expression in pachytene spermatocytes with age. For all images, high-DMRTB1-
875 expressing spermatocytes are indicated by diamond-headed arrows, while low-
876 DMRTB1-expressing spermatocytes are indicated by square-headed arrows.
877
878 **Figure 10** – *ATM and RAD51 have reduced expression in first-wave spermatocytes*
879 *from juvenile mice*. A) Spermatocyte marker SYCP3 (red) and ATM (green) were
880 stained in 5μm testis tissue sections from mice ages PND13, PND22, and adult. ATM
881 protein expression increases in SYCP3+ spermatocytes with age. For all images, high-
882 ATM-expressing spermatocytes are indicated by diamond-headed arrows, while low-
883 ATM-expressing spermatocytes are indicated by square-headed arrows.
884 B) Spermatocyte marker SYCP3 (red) and RAD51 (green) were stained in 5μm testis
885 tissue sections from mice ages PND13, PND22, and adult. RAD51 protein expression
886 increases in SYCP3+ spermatocytes with age. For all images, high-RAD51-expressing
887 spermatocytes are indicated by diamond-headed arrows, while low-RAD51-expressing
888 spermatocytes are indicated by square-headed arrows.
889

890 **Supplementary Figure 1** – *Similarities between "PND18pre" and "PND18" libraries.* A)
891 Germ and somatic cell composition by proportion and absolute cell number from
892 libraries "PND18pre" (pre-Percoll) and "PND18" (post-Percoll). B) tSNE representation
893 of all cells with >500 detected genes and >2000 UMIs. PND18 libraries are color-coded
894 while other libraries are greyed out. C) Cell counts for each cell type plotted in (A). As a
895 result of all of these similarities, the data derived from the libraries was combined for
896 analysis.
897
898 **Supplementary Figure 2** – *Quality control violin plots of single-cell data before and*
899 *after filtering.* A) Distribution of gene and UMI counts, and mitochondrial gene
900 percentage per library-of-origin, before and after data filtration. B) Distribution of gene
901 and UMI counts, and mitochondrial gene percentage per cell type.
902
903 **Supplementary Figure 3** – *Additional clustering of data, into computationally*
904 *determined clusters.* Representative clustering of all cells with >500 detected genes and
905 >2000 UMIs, based on most significant principal components, color-coded by cell
906 cluster.
907
908 **Supplementary Figure 4** – *Dot plot analysis of known gene expression markers based*
909 *on cluster and cell type*. A) Dot plot representation of known marker genes per cell
910 cluster determined in Figure S3. B) Dot plot representation of known marker genes per
911 cell type determined in Figure 2.
912

913 **Supplementary Figure 5** – *Representative germ cell marker expression in cells from all*
914 *libraries-of-origin*. tSNE plot of germ cells from all libraries, as well as tSNE plots of
915 notable germ cell marker gene expression.
916
917 **Supplementary Figure 6** – *GSEA enrichment plots for pathways correlated with*
918 *spermatogonia and spermatocyte development.* A) Enrichment plots for selected
919 Reactome database pathways in spermatogonia. Pathways
920 "SIGNALING_BY_SCF_KIT" and "SIGNALING_BY_FGFR" show negative correlation
921 with developmental time, while pathways "DESTABILIZATION_OF_MRNA" and
922 "SIGNALING_BY_WNT" show positive correlation with developmental time. B)
923 Enrichment plots for selected Reactome database pathways in spermatogonia. All
924 pathways shown demonstrate positive correlation with developmental time.
925
926 **Supplementary Figure 7** – *Split channels of ARSGL1 expression in spermatogonia*.
927 Spermatogonial marker PLZF (red) and ASRGL1 (green) were stained in 5μm testis
928 tissue sections from mice ages PND7, PND13, PND22, and adult. DAPI (blue) denotes
929 nuclei. ASRGL1 protein expression decreases in PLZF+ spermatogonia with age. High-
930 ASRGL1-expressing spermatogonia are indicated by full arrows with a line, while low-
931 ASRGL1-expressing spermatogonia are indicated by arrowheads. Individual channels
932 are represented in gray scale.
933
934 **Supplementary Figure 8** - *Split channels of ARSGL1 expression in spermatocytes*.
935 Spermatocyte marker SYCP3 (red) and ASRGL1 (green) were stained in 5μm testis

936 tissue sections from mice ages PND13, PND22, and adult. ASRGL1 protein expression
937 increases in SYCP3+ spermatocytes with age. For all images, high-ASRGL1-expressing
938 spermatogonia are indicated by full arrows with a line. Individual channels are
939 represented in gray scale.
940
941 **Supplementary Figure 9** – *RBMXL2 is highly expressed specifically in spermatogonia*
942 *from neonatal and juvenile mice, decreasing with age*. Spermatogonial marker PLZF
943 (red) and RBMXl2 (green) were stained in 5μm testis tissue sections from mice ages
944 PND7, PND13, PND22, and adult. DAPI (blue) denotes nuclei. RBMXL2 protein
945 expression decreases in PLZF+ spermatogonia with age. High-RBMXL2-expressing
946 spermatogonia are indicated by full arrows with a line, while low-RBMXL2-expressing
947 cells are indicated by arrowheads. Individual channels are represented in gray scale.
948
949 **Supplementary Figure 10** - *Split channels of DMRTB1 expression in spermatocytes.*
950 Spermatocyte marker SYCP3 (red) and DMRTB1 (green) were stained in 5μm testis
951 tissue sections from mice ages PND13, PND22, and adult. DMRTB1 protein is
952 expressed in the nucleus of first-wave spermatocytes at PND13, with decreasing
953 expression in pachyene spermatocytes with age. For all images, high-DMRTB1-
954 expressing spermatocytes are indicated by diamond-headed arrows, while low-
955 DMRTB1-expressing spermatocytes are indicated by square-headed arrows. Individual
956 channels are represented in gray scale.
957

958 **Supplementary Figure 11** – *Split channels of ATM expression in spermatocytes*.
959 Spermatocyte marker SYCP3 (red) and ATM (green) were stained in 5μm testis tissue
960 sections from mice ages PND13, PND22, and adult. ATM protein expression increases
961 in SYCP3+ spermatocytes with age. For all images, high-ATM-expressing
962 spermatocytes are indicated by diamond-headed arrows, while low-ATM-expressing
963 spermatocytes are indicated by square-headed arrows. Individual channels are
964 represented in gray scale.
965
966 **Supplementary Figure 12** – *Split channels of RAD51 expression in spermatocytes*.
967 Spermatocyte marker SYCP3 (red) and RAD51 (green) were stained in 5μm testis
968 tissue sections from mice ages PND13, PND22, and adult. RAD51 protein expression
969 increases in SYCP3+ spermatocytes with age. For all images, high-RAD51-expressing
970 spermatocytes are indicated by diamond-headed arrows, while low-RAD51-expressing
971 spermatocytes are indicated by square-headed arrows. Individual channels are
972 represented in gray scale.
973
974 **Table Legends**
975
976 **Table S1 -** *Genes expressed in specific germ cell types***.** Marker genes were determined
977 that distinguish different primary cell clusters. Up to 250 genes per primary cell type are
978 listed, with statistics from Seurat comparing expression in the marker-associated cell
979 type (X.1) to all other germ cells (X.2). Data for these genes are depicted as row-
980 normalized gene expression in individual cells in **Figure 3**.

981

982 **Table S2 -** *Genes with high counts in spermatids (filtered out)*. Due to contaminating
983 cell-free mRNA derived from lysed spermatids (detected only in samples in which
984 spermatids are present), these genes expressed at high levels in spermatids were
985 removed from the dataset. The UMI1/UMI2 ratio reflects the expression of each gene in
986 spermatids relative to all other germ cells.

987

988 **Table S3 -** *Genes with variable expression in spermatogonia during testis maturation.*
989 Model-based analysis of single-cell transcriptomics (MAST) was utilized to identify
990 genes that are variably expressed in spermatogonia as a function of mouse age. Genes
991 listed in this table include "markers" (genes with significantly upregulated expression in
992 all spermatogonia), as well as genes with significant variation in expression in
993 spermatogonia during testis maturation. Data for these genes are depicted as row-
994 normalized gene expression in individual cells in **Figure 4**.

995

996 **Table S4 -** *Gene Set Enrichment Analysis of Reactome pathways in spermatogonia*
997 *during testis maturation*. Reactome pathways with significantly differential expression as
998 a function of mouse age in spermatogonia are included (FDR < 0.05); the same results
999 are displayed in Cytoscape diagrams in **Figure 5**. The table includes GSEA results for
1000 each significant Reactome pathway, including the gene list, enrichment score (ES),
1001 normalized enrichment score (NES), and results of the statistical test for enrichment.

1002

1003 **Table S5 -** *Genes with variable expression in spermatocytes during testis maturation.*
1004 Model-based analysis of single-cell transcriptomics (MAST) was utilized to identify
1005 genes that are variably expressed in spermatocytes as a function of age. Genes listed
1006 in this table include “markers” (genes with significantly upregulated expression in all
1007 spermatocytes), as well as genes with significant variation in expression in
1008 spermatocytes during testis maturation. Data for these genes are depicted as row-
1009 normalized gene expression in individual cells in **Figure 6**.
1010
1011 **Table S6 -** *Gene Set Enrichment Analysis of Reactome pathways in spermatocytes*
1012 *during testis maturation.* Reactome pathways with significant differential expression as a
1013 function of mouse age in spermatocytes are included (FDR < 0.05); the same results
1014 are displayed in Cytoscape diagrams in **Figure 7**. The table includes GSEA results for
1015 each significant Reactome pathway, including the gene list, enrichment score (ES),
1016 normalized enrichment score (NES), and results of the statistical test for enrichment.
1017
1018 **Table S7** – *Antibodies used for immunofluorescent staining*. All primary and secondary
1019 antibodies used for immunofluorescence validation are documented with product
1020 numbers and dilutions used.
1021

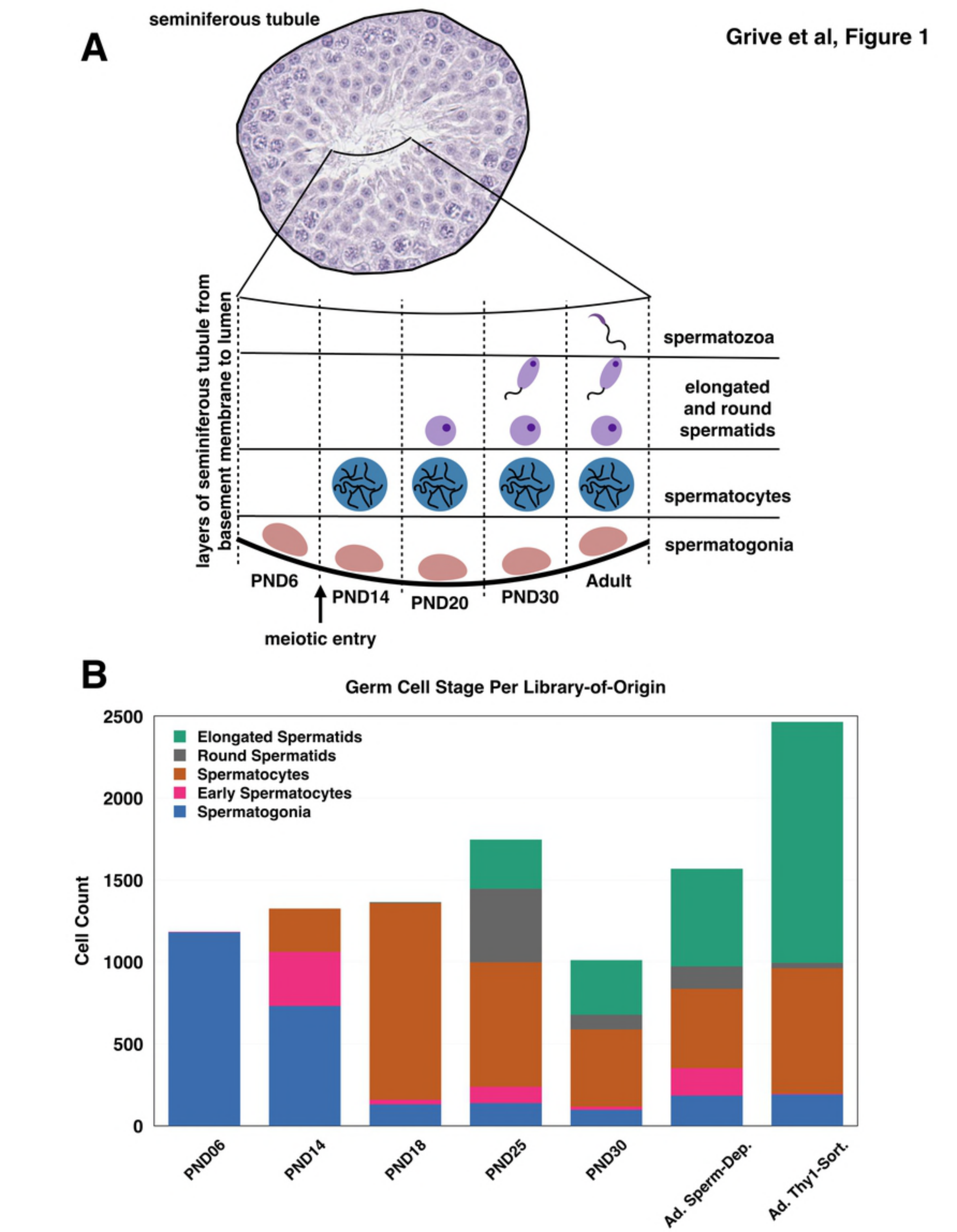
A
seminiferous tubule
Grive et al, Figure 1
layers of seminiferous tubule from basement membrane to lumen
spermatozoa
elongated and round spermatids
spermatocytes
spermatogonia
PND6
PND14
PND20
PND30
Adult
meiotic entry
B
Germ Cell Stage Per Library-of-Origin
Elongated Spermatids
Round Spermatids
Spermatocytes
Early Spermatocytes
Spermatogonia
Cell Count
2500
2000
1500
1000
500
0
PND06
PND14
PND18
PND25
PND30
Ad. Sperm-Dep.
Ad. Thy1-Sort.

Figure 1

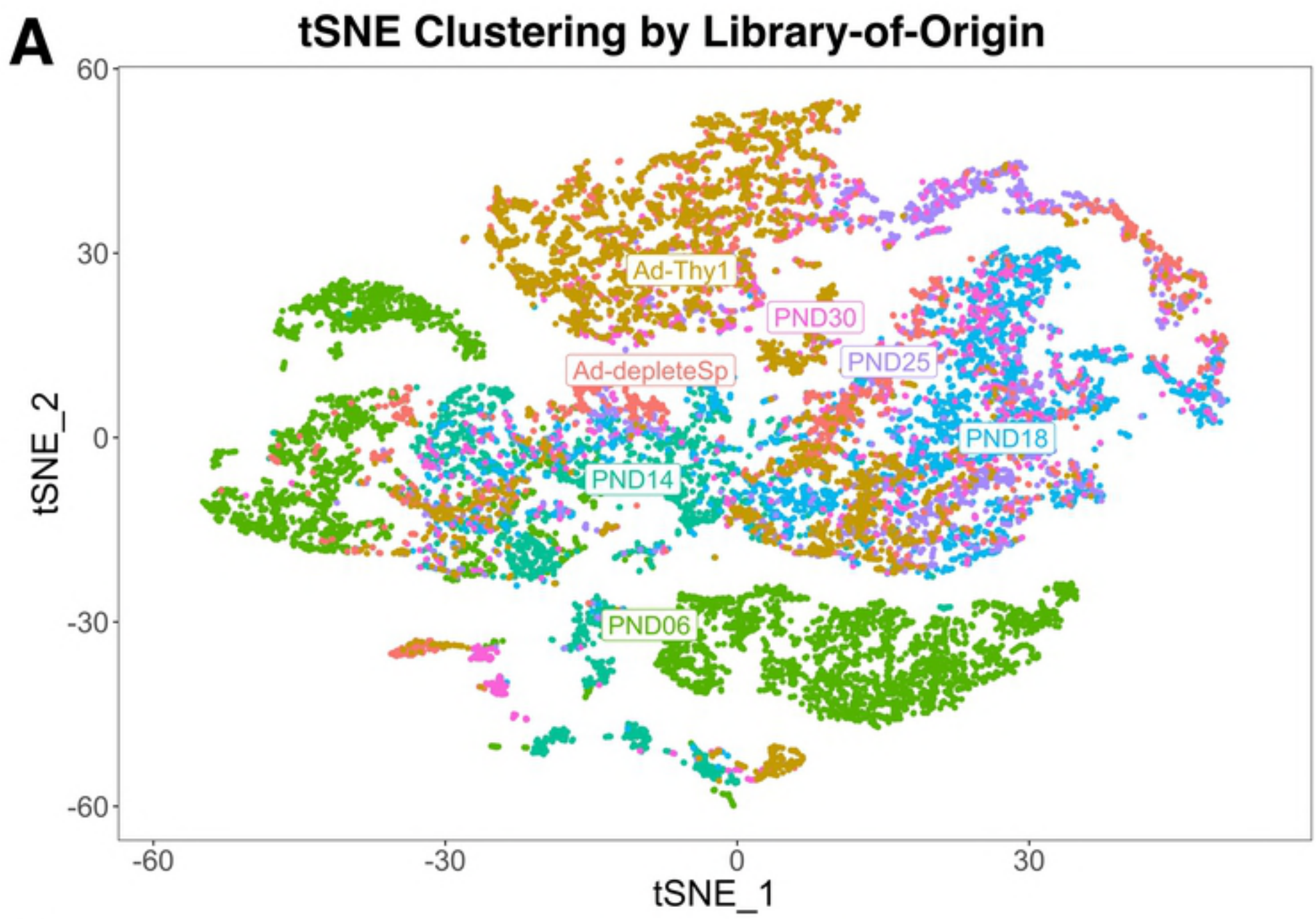
A
tSNE Clustering by Library-of-Origin
Ad-Thy1
PND30
PND25
Ad-depleteSp
PND18
PND14
PND06
tSNE_2
tSNE_1
60
30
0
-30
-60
-60
-30
0
30

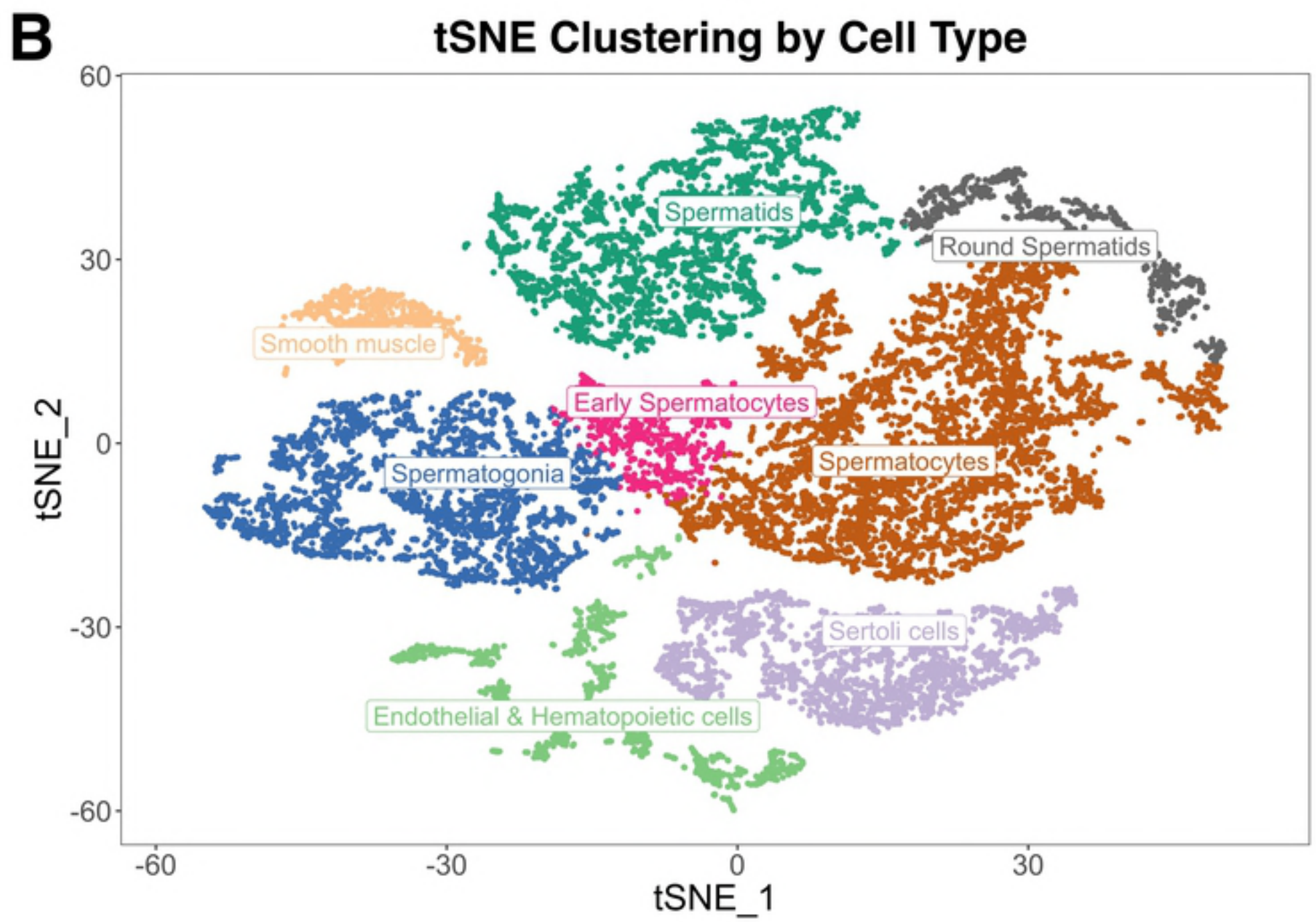
B
tSNE Clustering by Cell Type
Spermatids
Round Spermatids
Smooth muscle
Early Spermatocytes
Spermatogonia
Spermatocytes
Sertoli cells
Endothelial & Hematopoietic cells
tSNE_2
tSNE_1
60
30
0
-30
-60
-60
-30
0
30

Figure 2

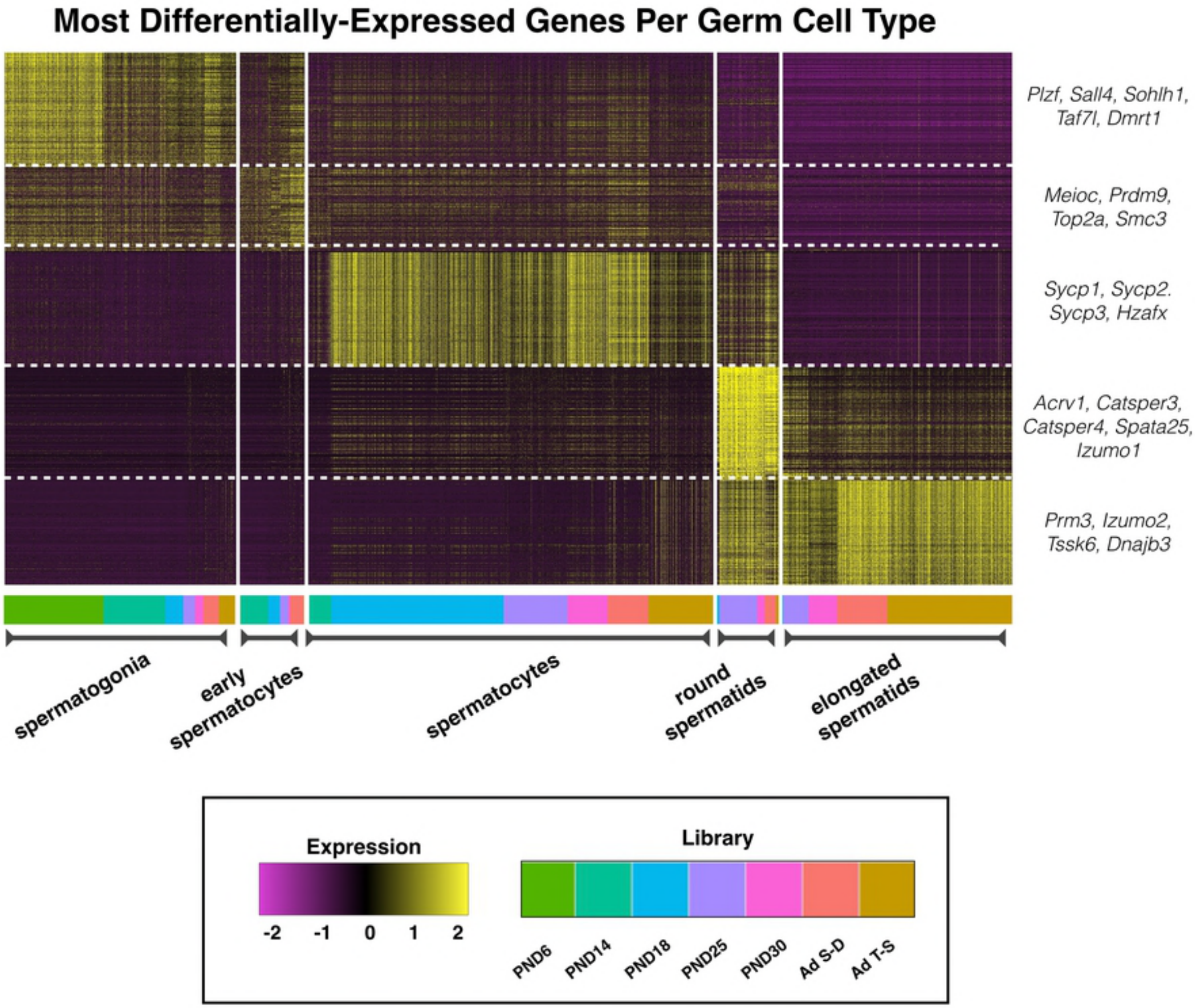
Most Differentially-Expressed Genes Per Germ Cell Type
Plzf, Sall4, Sohlh1, Taf7l, Dmrt1
Meioc, Prdm9, Top2a, Smc3
Sycp1, Sycp2. Sycp3, Hzafx
Acrv1, Catsper3, Catsper4, Spata25, Izumo1
Prm3, Izumo2, Tssk6, Dnajb3
spermatogonia
early spermatocytes
spermatocytes
round spermatids
elongated spermatids
Expression
-2
-1
0
1
2
Library
PND6
PND14
PND18
PND25
PND30
Ad S-D
Ad T-S

Figure 3

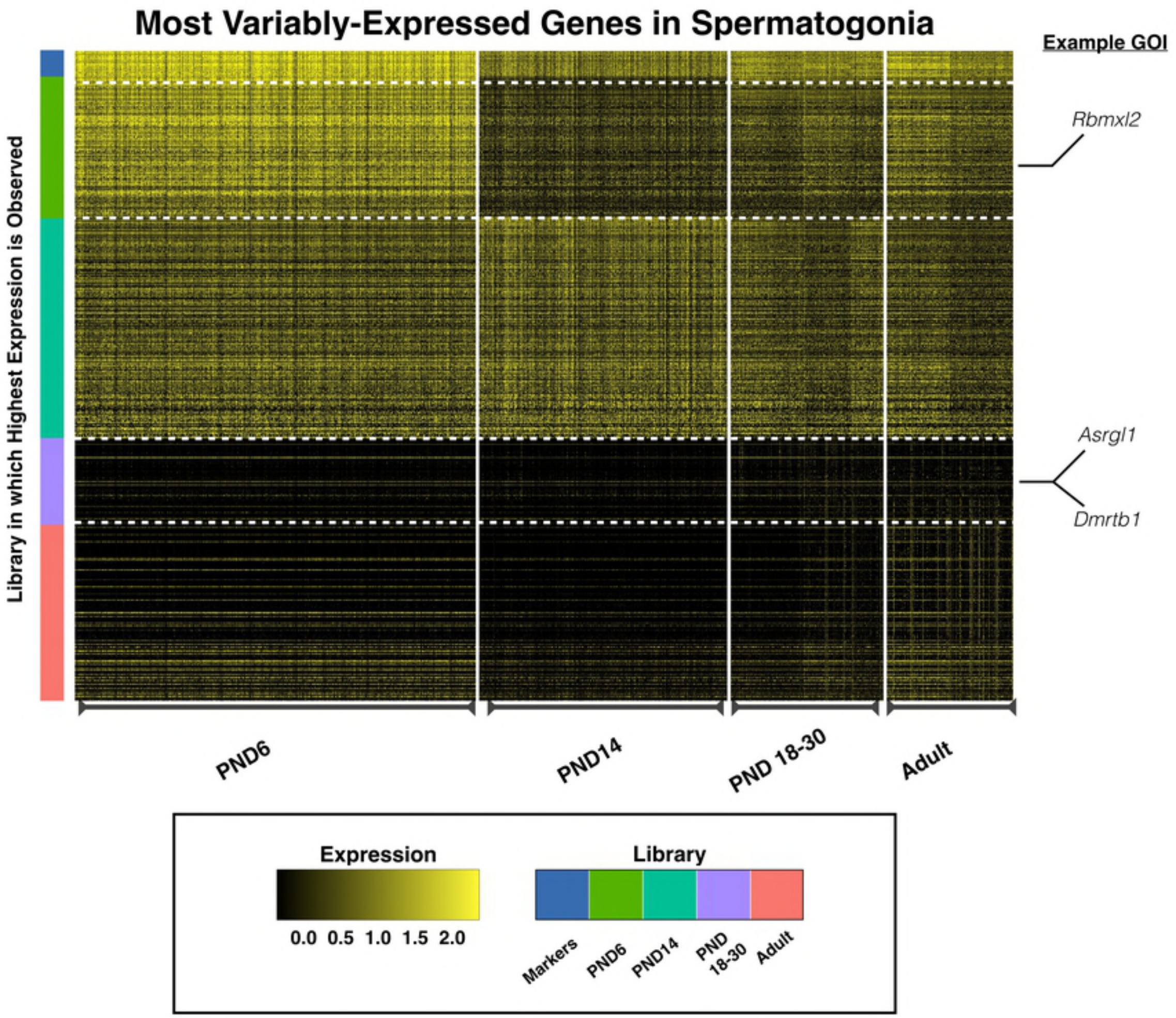
Most Variably-Expressed Genes in Spermatogonia
Example GOI
Rbmxl2
Asrgl1
Dmrtb1
Library in which Highest Expression is Observed
PND6
PND14
PND 18-30
Adult
Expression
0.0 0.5 1.0 1.5 2.0
Library
Markers
PND6
PND14
PND 18-30
Adult

Figure 4

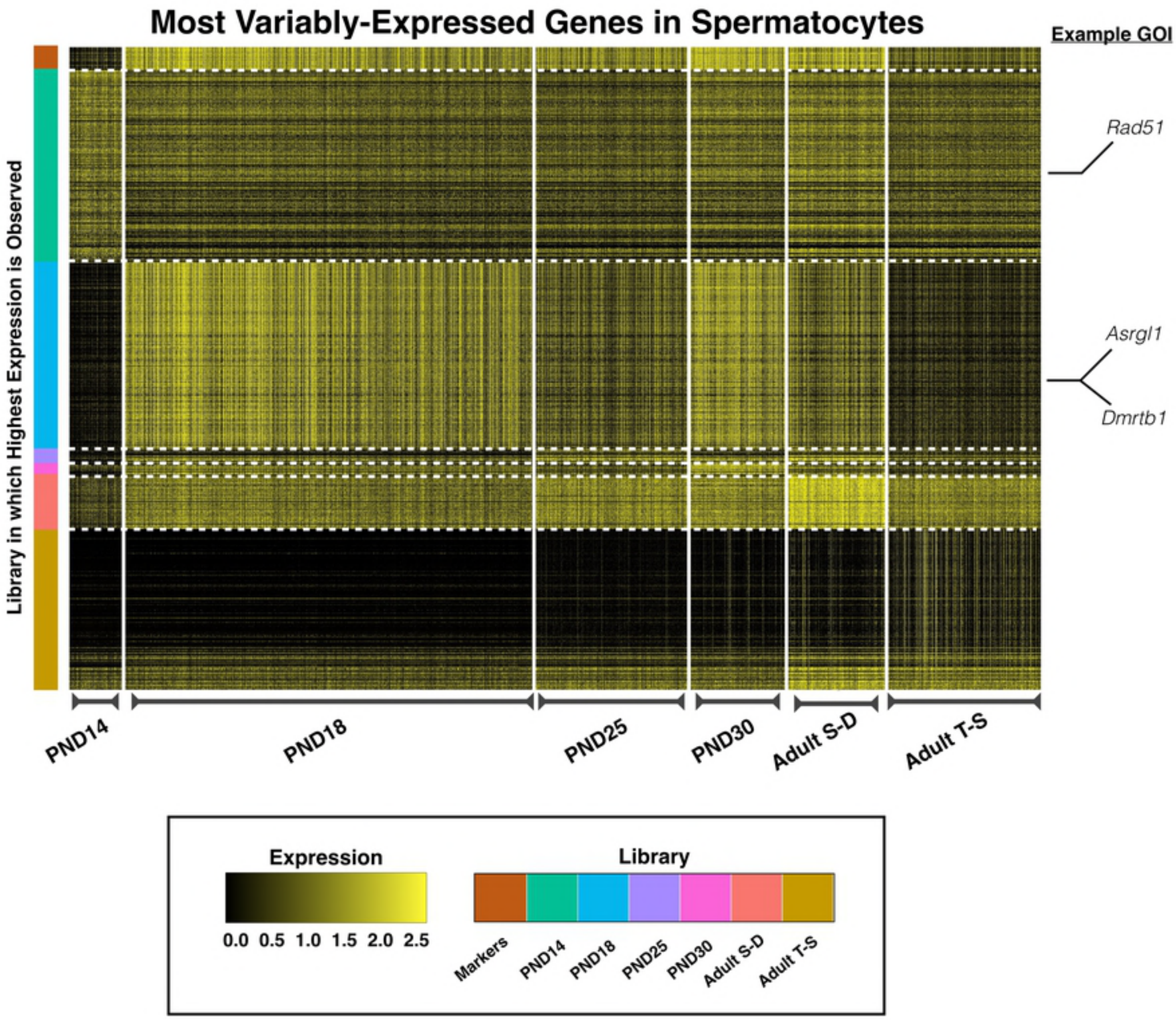
Most Variably-Expressed Genes in Spermatocytes
Example GOI
Rad51
Asrgl1
Dmrtb1
Library in which Highest Expression is Observed
PND14
PND18
PND25
PND30
Adult S-D
Adult T-S
Expression
0.0 0.5 1.0 1.5 2.0 2.5
Library
Markers
PND14
PND18
PND25
PND30
Adult S-D
Adult T-S

Figure 6

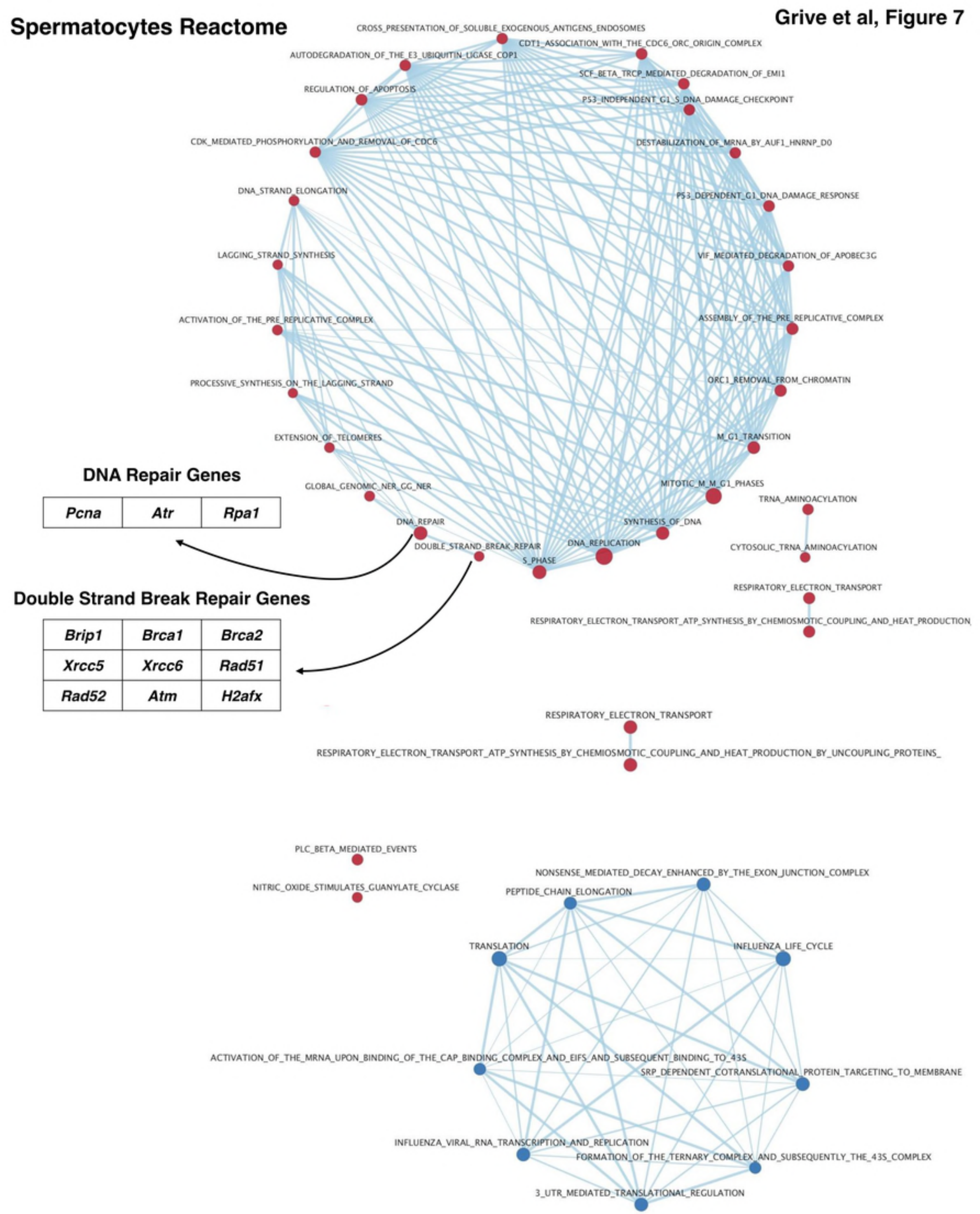
Spermatocytes Reactome
Grive et al, Figure 7
CROSS_PRESENTATION_OF_SOLUBLE_EXOGENOUS_ANTIGENS_ENDOSOMES
CDT1_ASSOCIATION_WITH_THE_CDC6_ORC_ORIGIN_COMPLEX
AUTODEGRADATION_OF_THE_E3_UBIQUITIN_LIGASE_COP1
SCF_BETA_TRCP_MEDIATED_DEGRADATION_OF_EMI1
REGULATION_OF_APOPTOSIS
P53_INDEPENDENT_G1_S_DNA_DAMAGE_CHECKPOINT
CDK_MEDIATED_PHOSPHORYLATION_AND_REMOVAL_OF_CDC6
DESTABILIZATION_OF_MRNA_BY_AUF1_HNRNP_D0
DNA_STRAND_ELONGATION
P53_DEPENDENT_G1_DNA_DAMAGE_RESPONSE
LAGGING_STRAND_SYNTHESIS
VIF_MEDIATED_DEGRADATION_OF_APOBEC3G
ACTIVATION_OF_THE_PRE_REPLICATIVE_COMPLEX
ASSEMBLY_OF_THE_PRE_REPLICATIVE_COMPLEX
PROCESSIVE_SYNTHESIS_ON_THE_LAGGING_STRAND
ORC1_REMOVAL_FROM_CHROMATIN
EXTENSION_OF_TELOMERES
M_G1_TRANSITION
DNA Repair Genes
GLOBAL_GENOMIC_NER_GG_NER
MITOTIC_M_M_G1_PHASES
TRNA_AMINOACYLATION
Pcna Atr Rpa1
DNA_REPAIR
SYNTHESIS_OF_DNA
DOUBLE_STRAND_BREAK_REPAIR
DNA_REPLICATION
CYTOSOLIC_TRNA_AMINOACYLATION
S_PHASE
RESPIRATORY_ELECTRON_TRANSPORT
Double Strand Break Repair Genes
RESPIRATORY_ELECTRON_TRANSPORT_ATP_SYNTHESIS_BY_CHEMIOSMOTIC_COUPLING_AND_HEAT_PRODUCTION
Brip1 Brca1 Brca2
Xrcc5 Xrcc6 Rad51
Rad52 Atm H2afx
RESPIRATORY_ELECTRON_TRANSPORT
RESPIRATORY_ELECTRON_TRANSPORT_ATP_SYNTHESIS_BY_CHEMIOSMOTIC_COUPLING_AND_HEAT_PRODUCTION_BY_UNCOUPLING_PROTEINS_
PLC_BETA_MEDIATED_EVENTS
NONSENSE_MEDIATED_DECAY_ENHANCED_BY_THE_EXON_JUNCTION_COMPLEX
NITRIC_OXIDE_STIMULATES_GUANYLATE_CYCLASE
PEPTIDE_CHAIN_ELONGATION
TRANSLATION
INFLUENZA_LIFE_CYCLE
ACTIVATION_OF_THE_MRNA_UPON_BINDING_OF_THE_CAP_BINDING_COMPLEX_AND_EIFS_AND_SUBSEQUENT_BINDING_TO_43S
SRP_DEPENDENT_COTRANSLATIONAL_PROTEIN_TARGETING_TO_MEMBRANE
INFLUENZA_VIRAL_RNA_TRANSCRIPTION_AND_REPLICATION
FORMATION_OF_THE_TERNARY_COMPLEX_AND_SUBSEQUENTLY_THE_43S_COMPLEX
3_UTR_MEDIATED_TRANSLATIONAL_REGULATION

Figure 7

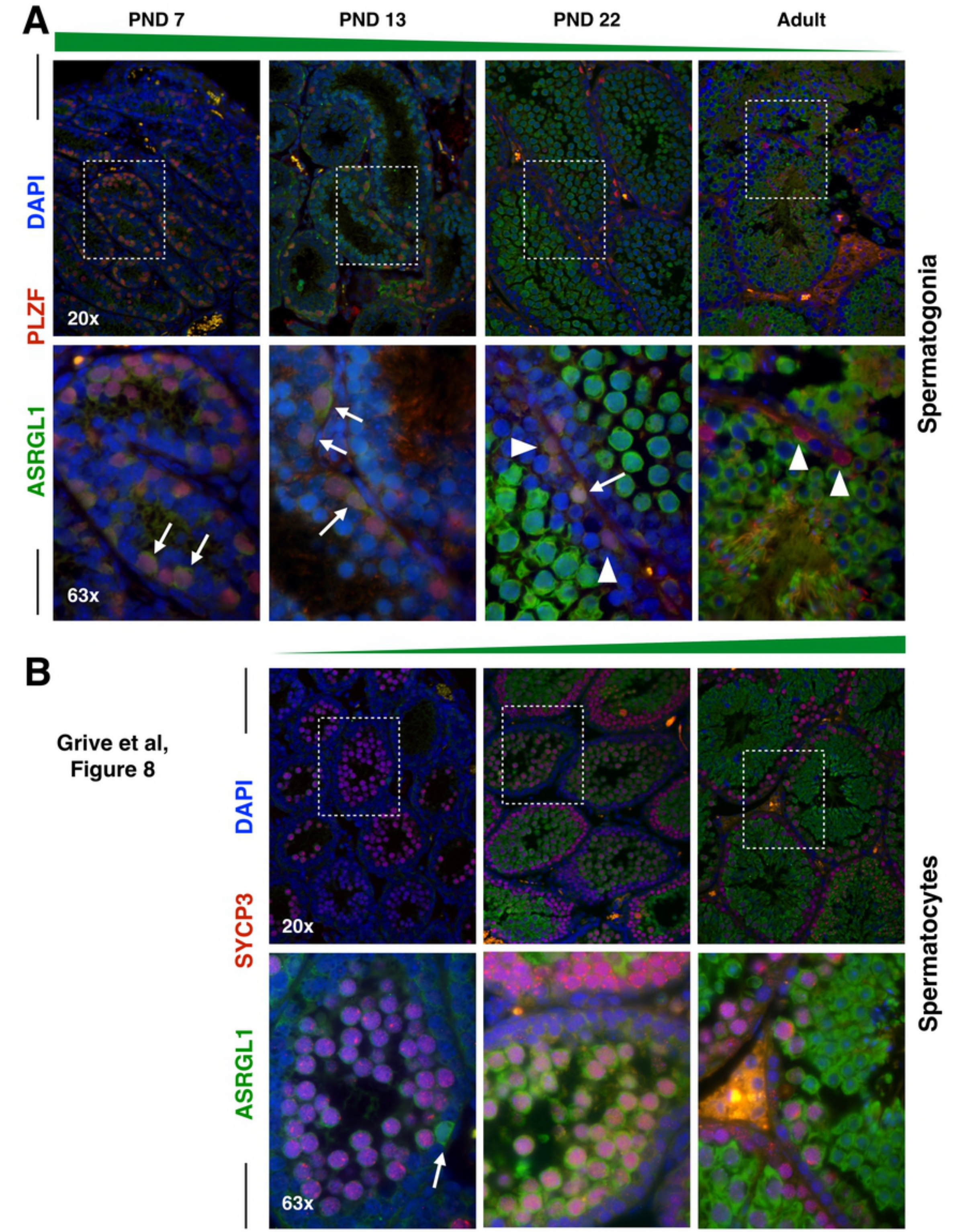
A
PND 7
PND 13
PND 22
Adult
DAPI
PLZF
ASRGL1
20x
63x
Spermatogonia
B
Grive et al,
Figure 8
DAPI
SYCP3
ASRGL1
20x
63x
Spermatocytes

Figure 8

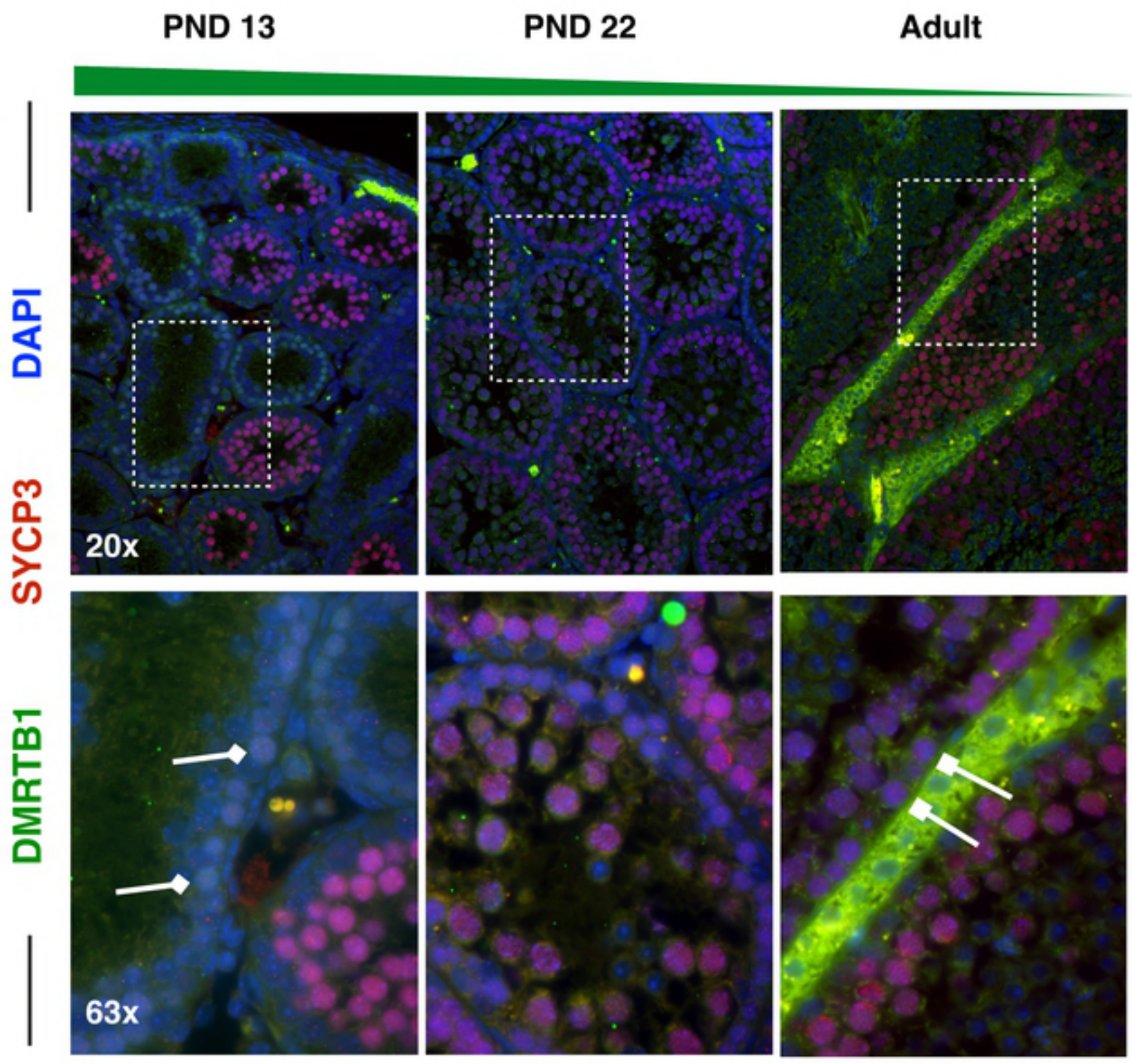

Figure 9

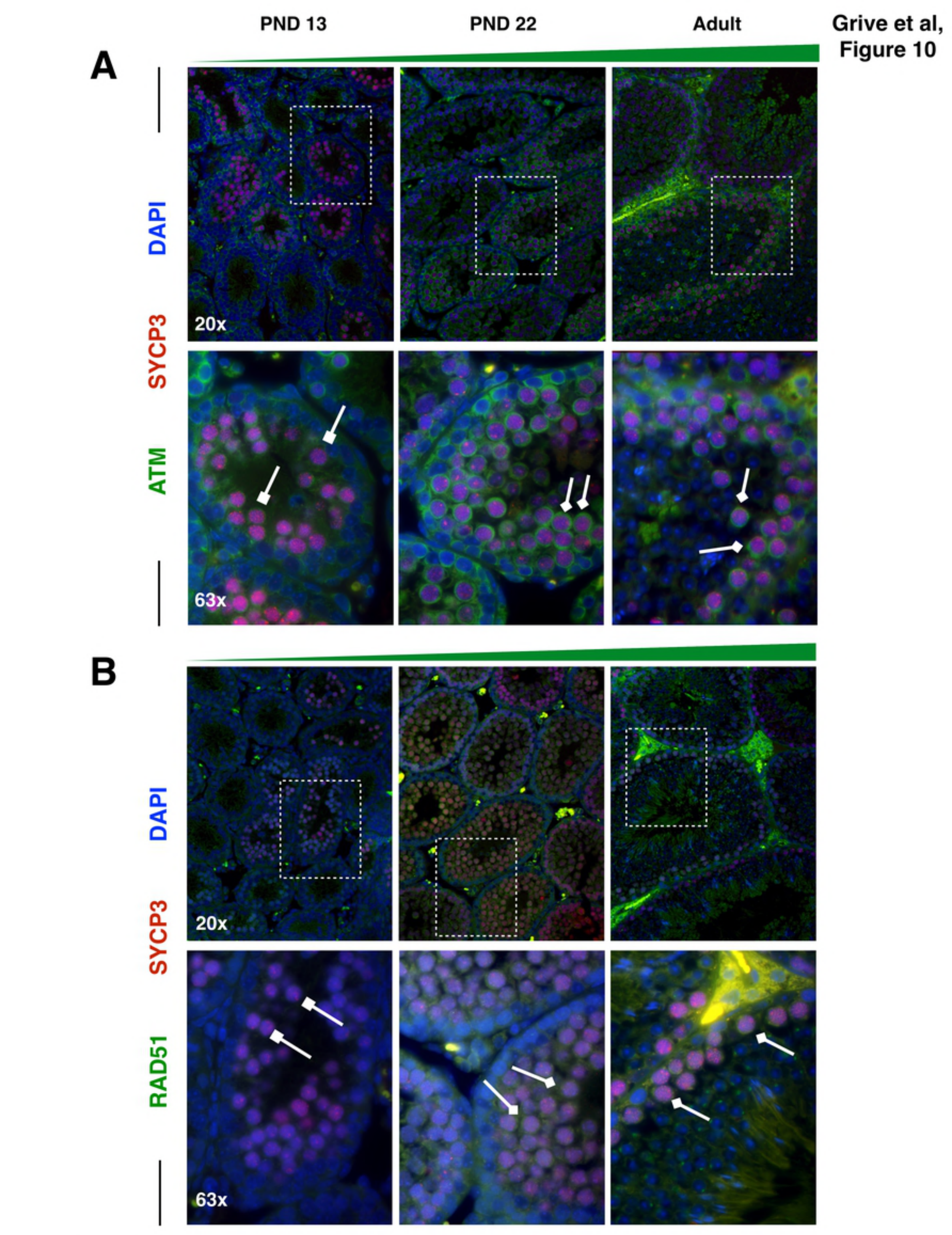
PND 13
PND 22
Adult
Grive et al,
Figure 10
A
DAPI
SYCP3
ATM
20x
63x
B
DAPI
SYCP3
RAD51
20x
63x

Figure 10

Spermatogonia Reactome

Grive et al, Figure 5

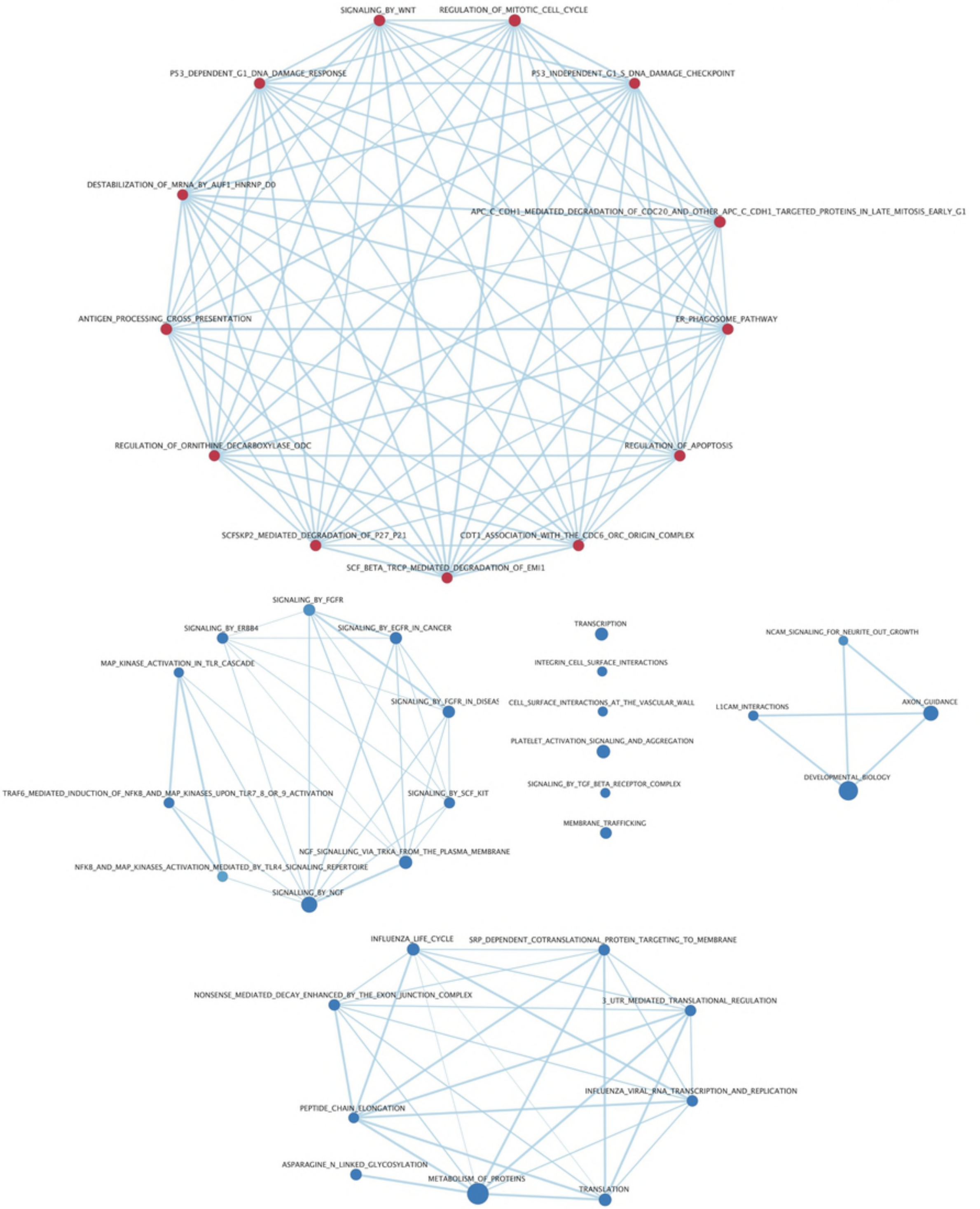

Figure 5